Modeling and Analysis of Wireless Cognitive Radio Networks: A Geometrical Probability Approach

by

Maryam Ahmadi
B.Sc., Iran University of Science and Technology, 2007
M.Sc., Amirkabir University of Technology, 2010

A Dissertation Submitted in Partial Fulfillment of the
Requirements for the Degree of

DOCTOR OF PHILOSOPHY

in the Department of Computer Science

Modeling and Analysis of Wireless Cognitive Radio Networks: A Geometrical Probability Approach

by

Maryam Ahmadi
B.Sc., Iran University of Science and Technology, 2007
M.Sc., Amirkabir University of Technology, 2010

Supervisory Committee

Dr. J. Pan, Supervisor
(Department of Computer Science)

Dr. K. Wu, Departmental Member
(Department of Computer Science)

Dr. T. A. Gulliver, Outside Member
(Department of Electrical and Computer Engineering)

Supervisory Committee

Dr. J. Pan, Supervisor
(Department of Computer Science)

Dr. K. Wu, Departmental Member
(Department of Computer Science)

Dr. T. A. Gulliver, Outside Member
(Department of Electrical and Computer Engineering)

ABSTRACT

Wireless devices and applications have been an unavoidable part of human lives in the past decade. In the past few years, the global mobile data traffic has grown considerably and is expected to grow even faster in future.

Given the fact that the number of wireless nodes has significantly increased, the contention and interference on the license-free industrial, scientific, and medical band has become severer than ever. Cognitive radio nodes were introduced in the past decade to mitigate the issues related to spectrum scarcity.

In this dissertation, we focus on the interference and performance analysis of networks coexisting with cognitive radio networks and address the design and analysis of spectrum allocation and routing for cognitive radio networks. Spectrum allocation enables nodes to construct a link on a common channel at the same time so they can start communicating with each other. We introduce a new approach for the modeling and analysis of interference and spectrum allocation schemes for cognitive radio networks with arbitrarily-shaped network regions.

First, for the first time in the literature, we propose a simple and efficient approach that can derive the distribution of the distance between an arbitrary interior/exterior reference point and a random point within an arbitrary convex/concave irregular

polygon. This tool is essential in analyzing important distance-related performance metrics in wireless communication networks.

Second, considering the importance of interference analysis in cognitive radio networks and its important role in designing spectrum allocation schemes, we model and analyze a heterogeneous cellular network consisting of several cognitive femto cells and a coexisting multi-cell network. Besides the cumulative interference, important distance-related performance metrics have been investigated, such as the signal-to-interference ratio and outage probability.

Finally, the spectrum allocation and routing problems in cognitive radio networks have been discussed. Considering a wireless cognitive radio network coexisting with a cellular network with irregular polygon-shaped cells, we have used the tools developed in this dissertation and proposed a joint spectrum allocation and routing scheme.

PREFACE

Below, is a list of publication accomplished during my PhD studies. The papers that are most related to this dissertation are briefly explained.

1) M. Ahmadi, F. Tong, L. Zheng, and J. Pan, "Performance analysis for two-tier cellular systems based on probabilistic distance models," IEEE INFOCOM, 2015.

   A two-tier cellular network consisting of macro and femto cells was considered in which the cells were assumed to have arbitrary polygon shapes. Based on the distance distributions associated with arbitrary polygons, the cumulative interference, the SIR, and the outage probability were analyzed.

2) M. Ahmadi and J. Pan, "Random distances associated with arbitrary triangles: A recursive approach with an arbitrary reference point," UVicSpace, 2014.

   Using a decomposition and recursion approach, the distance distributions from an arbitrary reference point to an arbitrary triangle were obtained.

3) M. Ahmadi and J. Pan, "Random distances associated with trapezoids," arXiv, 2013.

   The distribution of the distance between two random points within a trapezoid or between two neighbor trapezoids was derived.

4) M. Ahmadi, M. Ni, and J. Pan, "A geometrical probability-based approach towards the analysis of uplink inter-cell interference," IEEE GLOBECOM, 2013.

   The cumulative interference and SIR were analyzed in a cellular network consisting of hexagon-shaped cells.

5) M. Ahmadi, Y. Zhuang, and J. Pan, "Distributed robust channel assignment for multi-radio cognitive radio networks," IEEE VTC, 2012.

   A spectrum allocation scheme was proposed where the cognitive radio nodes take into consideration the interference imposed on primary users as well as the total interference in the secondary network.

6) M. Ahmadi and J. Pan, "Cognitive wireless mesh networks: A connectivity preserving and interference minimizing channel assignment scheme," IEEE PacRim, 2011.

Cognitive radio nodes try to select the best channel among all available channels such that the network interference is minimized. The problem was formulated as an integer linear programming problem.

7) J. Gui, M. Ahmadi, and F. Tong, "Dynamically constructing and maintaining virtual access points in a macro cell with selfish nodes," Journal of Systems and Software, 2015.

8) F. Tong, L. Zheng, M. Ahmadi, M. Ni, and J. Pan, "Modeling and analyzing duty-cycling, pipelined-scheduling MACs for linear sensor networks," IEEE TVT, 2015.

9) F. Tong, M. Ahmadi, J. Pan, L. Zheng, and L. Cai, "Geometrical distance distribution for modeling performance metrics in wireless communication networks," ACM MobiCom Poster, 2014.

10) S. Basu, M. Ahmadi, M. Ni, and J. Pan, "Locating primary users in cognitive radio networks by generalized method of moments," IEEE GLOBECOM, 2014.

11) F. Tong, L. Zheng, M. Ahmadi, M. Ni, and J. Pan, "Modeling duty-cycling MAC protocols with pipelined scheduling for linear sensor networks," IEEE/CIC ICCC, 2014.

12) F. Tong, M. Ahmadi, and J. Pan, "Random distances associated with arbitrary triangles: A systematic approach between two random points," arXiv:1312.2498, 2013.

13) J. Tao, L. Zhang, M. Ahmadi, L. Chang, J. Pan, and W. Chen, "Hexagonal clustering with mobile energy replenishment in wireless sensor networks," IEEE GLOBECOM, 2013.

14) L. Zhang, M. Ahmadi, J. Pan, and L. Chang, "Metropolitan-scale taxicab mobility modeling," IEEE GLOBECOM, 2012.

15) J. Tao, L. He, Y. Zhuang, J. Pan, and M. Ahmadi, "Sweeping and active skipping in wireless sensor networks with mobile elements," IEEE GLOBECOM, 2012.

16) M. Ahmadi, L. He, J. Pan, and J. Xu, "A partition-based data collection algorithm for wireless sensor networks with a mobile sink," IEEE ICC, 2012.

Contents

List of Tables

List of Figures

List of Abbreviations

4G ..... Fourth-Generation Mobile Telecommunications Technology

5G ..... Fifth-Generation Mobile Telecommunications Technology

BS ..... Base Station

CAODV ..... Cognitive Ad hoc On Demand Vector routing

CAP ..... Channel Availability Probability

CCC ..... Common Control Channel

CDF ..... Cumulative Distribution Function

CTS ..... Clear To Send

D2D ..... Device-to-Device

FBS ..... Femto Base Station

FCC ..... Federal Communications Commission

FU ..... Femto User

ISM band .... Industrial, Scientific, and Medical radio band

MAC ..... Media Access Control

MBS ..... Macro Base Station

MU ..... Macro User

PDF ..... Probability Distribution Function

PPP ..... Poisson Point Process

RREQ ..... Route REQuest

RTS ..... Request To Send

PU ..... Primary User

SINR ..... Signal-to-Interference-and-Noise Ratio

SIR ..... Signal-to-Interference Ratio

SPR ..... Shortest Path Routing

SU ..... Secondary User

VANET ..... Vehicular Ad hoc NETwork

WLAN ..... Wireless Local Area Network

WSN ..... Wireless Sensor Network

ACKNOWLEDGEMENTS

I would like to start by expressing my appreciation to my lovely family. Thank you to my spouse, Andrew, for his love, support, and encouragement. Thank you for being so understanding and supportive through difficult days during my PhD studies. I want to thank my wonderful parents Mousa and Zahra, my brothers Amir and Nader, and my sister Mina. I am fortunate to have them as my family with never-ending love and support. I am the person I am today only because of them. It was very difficult being thousands of kilometres away from them for years, but I felt I was always loved and understood.

Thanks to Professor Jianping Pan for guidance and financial support during my PhD studies. Thanks to Professor Kui Wu and Professor T. Aaron Gulliver for serving as my committee members and providing constructive feedback and interesting ideas. My appreciation goes to Professor Ulrike Stege and Professor Micaela Serra for their incredible support.

I would like to express my appreciation to my current manager, Chris Lefebvre, at Nokia. I am thankful for his support, understanding, trust, and always giving me invaluable advice regarding my career, studies, and life.

DEDICATION

To

My spouse **Andrew**
My parents **Mousa and Zahra**
My siblings **Amir, Nader, and Mina**

Chapter 1

Introduction

1.1 Overview

In this dissertation, we focus on the interference and performance analysis of cognitive radio networks and address the design and analysis of spectrum allocation and routing for these networks

Aiming at providing a more realistic model, in contrary to the existing work, we consider network regions in the shape of complex geometries. Further, since the locations and distances among the transmitting, receiving, and interfering nodes have a considerable effect on wireless signals, in this dissertation, we derive the distance distributions associated with complex geometries, which are then used to analyze the interference in the network. The obtained distance distributions also assist us in designing a spectrum allocation scheme for cognitive radio networks.

1.2 Background

In the past decade, we have witnessed a significant increase of attention and interest in wireless applications, which have been made possible by the constant improvements in the wireless communication technologies. Nowadays, people's lives depend on the services provided by wireless communication networks, such as cellular services including data, voice, video, etc.

In terms of the network structure, wireless communication networks can either operate with the help of a central unit, in which case they are called infrastructure-based networks, or could form and operate without the assistance of a central unit, in

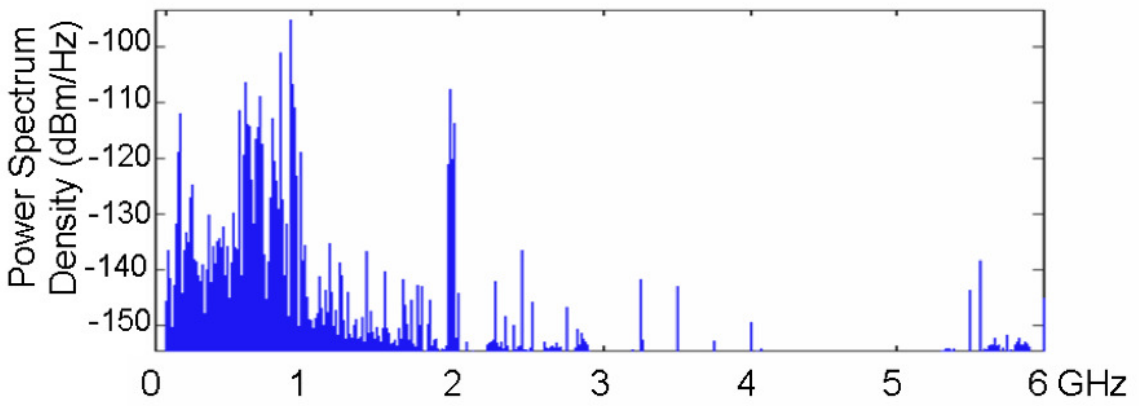

Figure 1.1: Measurement of the Spectrum Utilization for 0–6 GHz [49].

which case they are referred to as infrastructure-less or ad hoc networks. Examples of the former include cellular networks, Wireless Local Area Networks (WLANs), etc., and those of the latter are Wireless Sensor Networks (WSNs), Vehicular Ad hoc NETworks (VANETs), etc. The research done in this dissertation considers both infrastructure-based and infrastructure-less ad hoc networks.

Some wireless networks, such as WSNs, perform their transmissions over the unlicensed Industrial, Scientific, and Medical (ISM) band. However, with the huge increase in the number of the wireless applications and devices using this band, it has become extremely crowded where contention and interference have become important issues. Statistics and predictions show that the number of wireless devices and applications will continue to grow in the future [1]. As a result, scientists and researchers have been investigating possible solutions to accommodate the ever-increasing need for spectrum.

Investigations show that the ISM band is very crowded and many users are actively utilizing it, while other licensed bands are not occupied at all times [12]. Figure 1.1 shows the utilization of the spectrum between 0 and 6 GHz at downtown Berkeley [49]. As can be seen in the figure, some portions of the spectrum are heavily used, while other parts are moderately or sparsely used. Specifically, the spectrum holes (where the licensed spectrum is not in use) can be found in time, frequency, and location, and could be used by unlicensed users.

In 2008, the Federal Communications Commission (FCC) approved the use of licensed spectrum by unlicensed users only if their transmissions do not cause harmful interference with those of license-holders [3]. License-holders are also referred to as primary users, while unlicensed users are called secondary users. From the terms,

it is understood that primary users have priority for using the licensed spectrum, while secondary users can only use the licensed spectrum in an opportunistic way. Specifically, a secondary user can use licensed spectrum if a specific frequency is not being used by a primary user at a specific time, or if the specific channel is used by primary users but the secondary user is located far enough so that its transmissions would not cause harmful interference to the primary users that could be using the licensed channel simultaneously.

Cognitive radio networks were introduced as a solution to the spectrum scarcity problem. Cognitive radio users are capable of observing the environment, finding the available primary channels, switching to those channels, utilizing them, and leaving them once required by the primary users. Cognitive nodes are required to leave the spectrum as soon as a primary user appears on the same channel, as according to the regulations, they are only allowed to use the licensed spectrum as long as their transmissions do not interfere with primary user transmissions.

Since the introduction and development of cognitive radio technology, many practical and important issues have attracted the attention of the researchers. Spectrum sensing, spectrum allocation, routing, Media Access Control (MAC) layer protocols, etc., are some of the issues specific to cognitive radio networks, or their requirements have changed compared to traditional wireless communication networks. In general, how to realistically model and analyze cognitive radio networks and address the associated problems is still under research and development.

Transmissions in wireless communication networks are carried by the radio spectrum. Unlike traditional wired networks in which transmissions were directed towards the receiver using a physical medium, in wireless networks, the signal is propagated over the air. As a result, the signal is subject to noise and interference from other nodes that transmit simultaneously over the same frequency. The signal is also affected by different physical phenomena that are not avoidable.

Path loss phenomenon is one of the most important factors that affects the transmitted signals. Due to path loss, the transmitted signal could considerably attenuate with respect to the distance between the transmitter and the receiver. In other words, the received signal power will not be as strong as that of the transmitted signal. Besides path loss, other factors such as shadowing, fading, etc., can affect the transmitted signals.

The locations and distances among nodes have considerable impacts on the wirelessly transmitted signals. As a result, a mathematical tool that can efficiently char-

acterize the distances among wireless nodes is essential. As an example, the path loss, specifically, depends on the distance between the transmitter and receiver. In this dissertation, we focus on path loss, however, shadowing and fading can be easily incorporated in our model if they are not distance-related.

Besides the geometrical probability approach used in this dissertation, stochastic geometry is another mathematical tool that has been widely used for the modeling and analysis of wireless networks. Stochastic geometry usually is based on the assumption of an infinite network with an infinite number of nodes. Performance metrics for a typical node are obtained without dependence on the location of the node. However, with the geometrical probability approach, the locations of the nodes is taken into consideration, the border effect is carefully considered, and thus finite network regions can be modeled. Further, for networks where the locations of the nodes are not completely random, e.g., the locations of base stations are usually planned and determined before deployment, geometrical probability approach is preferred. In other words, stochastic geometry can be used to obtain results over different realizations of the network, while geometrical probability approach can give us insights about a specific snapshot of a network. For further discussions on the differences between geometrical probability and stochastic geometry approaches and a brief literature review, please refer to Chapter 3.

In order to model and analyze the coexistence of a primary network with cognitive radio networks and their effect on the performance of one another, the strengths of the transmitted signals in the primary network and the cognitive radio network, as well as the interference from one node to another, need to be considered. That would enable us to analyze the signal-to-interference ratio and other important performance metrics such as the outage probability.

In this dissertation, we investigate the distance-related parameters and metrics, such as the strengths of the signal and cumulative interference, Signal-to-Interference Ratio (SIR), outage probability, as well as their application in spectrum allocation and routing scheme design in cognitive radio networks.

1.3 Motivation and Contributions

In cognitive radio networks, the strength of the received signal and interference plays important roles in determining which primary channels can be utilized by secondary users. These important performance metrics, such as the strength of the interference

signal, SIR, outage probability, etc., are all functions of the distances among nodes. Specifically, they depend on the locations of the nodes and the distances among them.

Primary network nodes and cognitive radio users are assumed to be distributed in a certain network region following a given distribution. As a result, given the locations of the nodes and the shape of the network region, the distribution of the distances among nodes can be obtained.

The contributions of this dissertation are threefold. First, from the geometrical probability point of view, we derive the distribution of the distance between an arbitrary reference node and a random node within an irregular polygon. Second, considering a network where nodes are distributed in irregular-shaped network regions, we analyze important location-critical metrics such as the received signal strength, cumulative interference, the SIR, and the outage probability. Third, using the tools and results developed, a joint spectrum allocation and routing scheme for a cognitive radio network is designed. The location of the nodes as well as the distances among them are taken into consideration when designing a spectrum allocation and routing scheme for cognitive radio networks.

1.3.1 Distance Distributions to an Arbitrary Polygon from an Arbitrary Reference Point

Aiming at modeling and analyzing a network with more realistic region shapes, we assume that nodes are distributed in an irregular polygon-shaped region. Existing work has considered network regions of regular shapes, such as circles, squares, rhombuses, hexagons, etc. However, due to the complicated factors that affect signal propagation in wireless environments, the coverage area of a network is likely not a regular shape. Thus, in this dissertation, we consider wireless networks with irregular polygon shapes.

Since many of the important performance metrics depend on the locations of the nodes and the distances among them, in Chapter 2 of this dissertation, we focus on obtaining the distribution of the distances between nodes that are distributed in an irregular polygon. Specifically, we are interested in distance distributions from an arbitrary reference point. For the first time in the literature, we propose a scheme that can handle the cases where the arbitrary reference point is either inside or outside the network region. Further, the network area where nodes are distributed can be a convex or concave irregular polygon.

We propose a decomposition and recursion approach to obtain the distance distributions from an arbitrary reference point. Regardless of an interior or exterior reference point, the irregular polygon is first decomposed into triangles. Note that since the polygon is irregular, the formed triangles are likely irregular as well. Thus, the problem is simplified to obtaining the distance distributions from the given reference point to all the triangles that form the polygon. At the last step, a probabilistic summation is done to obtain the Probability Distribution Function (PDF) of the distance between the reference point and the whole polygon. In Chapter 2, we explain in detail how the decomposition and recursion approach works.

1.3.2 Performance Analysis for a Heterogeneous Cognitive Radio Network

Based on current statistics and predictions for growth of data traffic in the next few years, the researchers and industry partners have been working on finding solutions to handle the huge amount of data traffic. A 5G cellular network is proposed as a solution to obtain 1000-fold aggregate data rate through different methods, one of which is extreme densification [13]. This solution is proposed to reduce the size of the cells in order to serve more users per area by reusing the spectrum across a geographical area. This approach ensures the reduction in the number of the nodes that are competing to communicate with the base station. Furthermore, a large amount of data traffic is originated from indoor environments where the cellular coverage is poor. Similarly, deploying small low-power base stations with smaller coverage areas (a.k.a. femto base stations) can reduce the size of the cells and the number of served users. That in turn improves the cellular service quality in indoor environments such as homes and offices, and reduces the cost through using lower-power and cheaper base stations. Despite the fact that femto cells can considerably improve the quality of service for indoor users, if densely deployed, they could be harmful to the cellular network base stations and users. The reason is that the cumulative interference caused by the femto devices could negatively affect the transmitted cellular signals.

In Chapter 3, we consider a multi-cell cellular network consisting of irregular-shaped cells. There is a base station in each macro cell. In addition, multiple femto cells are deployed in each macro cell to efficiently serve the indoor users. Using the distribution of the distances associated with arbitrary polygons as obtained in Chapter 2, we analyze the cumulative interference from femto cells to the cellular base

station. Besides the cumulative interference, we have analyzed important performance metrics such as the signal-to-interference ratio and the outage probability.

1.3.3 Spectrum Allocation in Cognitive Radio Ad Hoc Networks

To address the spectrum scarcity problem, since 2008, FCC allows unlicensed users, a.k.a. cognitive radio users, to utilize the licensed spectrum as long as their transmissions would not cause harmful interference on those of licensed users, a.k.a. primary users.

Since the idea of cognitive radio technology was introduced, many important research problems have appeared. In Chapter 4, we focus on the spectrum allocation problem. Spectrum allocation addresses the important problem of assigning frequency channels to cognitive radio nodes with respect to the licensed channel availability, which enables the cognitive users to communicate with each other once they are on the same channel at the same time.

We propose to probabilistically measure the probability that a licensed channel is available to cognitive users. Similarly, we obtain the probability that a link can be established between two neighboring cognitive radio users. This probability is derived from the activity patterns of the primary users as well as the interference analysis. Since interference strongly depends on the distances between the interfering nodes, we have utilized the distributions of the random distances obtained in Chapter 2 of this dissertation to characterize the interference between nodes.

The link availability probabilities are incorporated into the spectrum allocation and routing procedures in cognitive radio networks. A metric based on such probabilities is defined to characterize the expected time needed for a successful multi-hop transmission. The simulation results show that the network performance can be improved, in terms of the end-to-end delay and throughput, when the proposed metric is taken into consideration in designing spectrum allocation and routing schemes.

1.4 Outline of the Dissertation

The rest of this dissertation is organized as follows. In chapter 2, a mathematical tool for obtaining the distance distributions from an arbitrary reference point to a convex or concave arbitrary polygon is presented. In Chapter 3, the interference and

performance analysis is done for a cellular network coexisting with multiple cognitive femto cells. Based on the interference analysis, a joint routing and spectrum allocation scheme for cognitive radio networks is proposed in Chapter 4. Conclusions and future directions are in Chapter 5.

Chapter 2

Distance Distributions to an Arbitrary Polygon from an Arbitrary Reference Point

2.1 Overview

As explained in Chapter 1, interference analysis plays an important role in the design of efficient spectrum allocation schemes. In wireless communication networks, the received signal power is a function of the distance between the receiver and the transmitter. Similarly, the interference power depends on the distance between the location where the interference is measured and the interferers. As a result, in this chapter, we focus on obtaining the distribution of the distance between an arbitrary interior/exterior reference point to a random point within an arbitrary convex/concave polygon. We give detailed numerical and simulation results to show the accuracy of our approach. Further, a few case studies are discussed to demonstrate how our results can be used in practical wireless networking research scenarios. In the following chapters, we will show how these results will help with the interference analysis as well as design and analysis of spectrum allocation schemes for cognitive radio networks. Parts of the work in this Chapter were previously presented in [8].

2.2 Introduction

Many of the performance metrics in wireless networks, e.g., interference, outage probability, connectivity, etc., can be characterized based on the distances between the nodes. Let us give a simple example of interference analysis in cellular networks. Due to path loss, the signal power attenuates with respect to the distance between the transmitter and the receiver. As a result, in order to analyze the total interference received at the base station from randomly located cellular users, the distance distributions between the base station and a randomly located transmitter in a cell can be utilized to characterize the cumulative interference from such nodes [6, 54]. Further, given the distributions of the received signal and interference power, other important metrics such as the Signal-to-Interference-and-Noise Ratio (SINR) and the outage probability can be obtained.

In previous existing work on the interference analysis and outage probability, for the sake of simplicity and analytical tractability, an infinite network was taken into consideration [19,46,48]. Furthermore, many of these papers assumed that the spatial distribution of the nodes follows a homogeneous Poisson Point Process (PPP). These assumptions simplify the performance analysis and modeling of the wireless network, but are unrealistic. For example, in these models, the mean interference is the same for all nodes in the network due to the underlying PPP model of the node distribution and the infinitely large network region.

However, many real world wireless networks consist of a finite number of nodes located within a finite region, and thus the above assumptions are not accurate. Unlike infinite networks with a PPP node distribution, in finite networks, network characteristics such as the interference depend on the location of each node as well as the network region shape. Unlike infinite networks, modeling and analysis of finite networks is very difficult and directly depends on the shape of the network region. Besides the shape, the location of the reference point, e.g., where the interference is being measured, has to be taken into consideration.

In many previous existing work on finite networks, for the ease of modeling and analysis, regular shape cells were assumed [6,54]. Cell shapes such as disks, rectangles, equilateral triangles, and hexagons, result in tractable analysis, while they may not model the real-world networks accurately. Given that signal attenuation depends on many different parameters according to the environment, the coverage area of a base station node is likely irregular. This fact emphasizes the need for deriving the

distance distributions associated with irregular shapes.

Motivated by the importance of having the distance distributions associated with arbitrary polygons [1], for the modeling and analysis of finite networks, we propose a decomposition and recursion approach that can be applied to finite network regions with any arbitrary polygon shape, as well as any location of the reference point. With our approach, for the first time in the literature, the inter-cell interference can be analyzed for arbitrarily-shaped finite networks. Previously, no approach was able to obtain the distribution of the distance from an exterior reference point, i.e., when the interferers are located in another cell.

Our main contributions are as follows. First, using the proposed decomposition and recursion approach, we solve the problem of obtaining distance distributions to arbitrary triangles from an arbitrary reference point. Our proposed approach while very effective and generic, consists of simple mathematical tools and solves an important problem that was unsolved for decades. Second, by extending the decomposition and recursion approach, distance distributions from interior/exterior arbitrary reference points to arbitrary polygons are derived. In the next chapter, we will show in detail how the proposed approach and results in this chapter can be applied to a practical scenario where the SIR and the outage probability for a BS in a heterogeneous network are obtained.

2.3 Related Work

The problem of obtaining the inter-node distance distributions can be divided into two categories: 1) the distance distribution between two random nodes, and 2) the distribution of the distance between an arbitrary reference node and a random node. In [9, 55, 56, 58], the authors derived the distance distributions between two randomly located nodes within one and between two neighbor regular rhombuses, hexagons, equilateral triangles, and trapezoids, respectively. The distance distributions between two random nodes within an arbitrary triangle were derived in [44] which is a leap forward as the approach does not have any constraints on the shape of the triangle. Moreover, our work in [44] is extended to arbitrary polygons according to the fact that every polygon can be triangulated, solving all cases regarding the distance distributions between two random nodes.

[1] Arbitrary means the shape could be regular or irregular and convex or concave.

On the other hand, the distribution of the distance from a reference point has been discussed in some of the existing literature. The distance distributions between a random point in a disk to an arbitrary reference point were given in [36]. The distance distributions between a random point in a square to its center, vertices, and midpoint of sides were obtained in [39]. [35] gives the distance distribution from a vertex of a triangle, however, the approach does not cover arbitrary triangles. For regular hexagons, such distance distributions from the center of the same or an adjacent hexagon were discussed in [54] based on the area-ratio approach. The results in all these papers, however, are limited to regular shapes and specific locations of the reference point. The distance distributions from an interior reference point to a hexagon were covered in [14] along with analytical and approximated expressions for path loss.

In a more recent work, the distance distributions from an arbitrary interior point to a random point within any regular polygon were obtained [31]. Their approach is general in the sense that it applies to any regular polygon, however, it is limited to interior reference points only.

Different from the existing work, we propose a generic approach that can solve all cases regarding the distance distributions to an arbitrary convex/concave polygon from an arbitrary interior/exterior reference point [2].

2.4 Problem Statement

The problem addressed in this chapter is obtaining the distance distribution from an arbitrary reference point to a random point within an arbitrary polygon. Due to the fact that every polygon can be decomposed into triangles, by employing a decomposition and recursion scheme, the distance distributions to arbitrary polygons can be obtained based on those to arbitrary triangles, as explained and demonstrated in Section 2.6. Thus, we first focus on the fundamental problem of deriving the distance distribution from an arbitrary reference point to a random point within an arbitrary triangle.

[2] [40] also solves the problem of obtaining distance distributions from an arbitrary reference point to arbitrary polygons, however, the authors have borrowed the approach for obtaining the distance distributions to arbitrary triangles proposed in this dissertation. They have used a modified form of the shoelace formula [5] to extend our results.

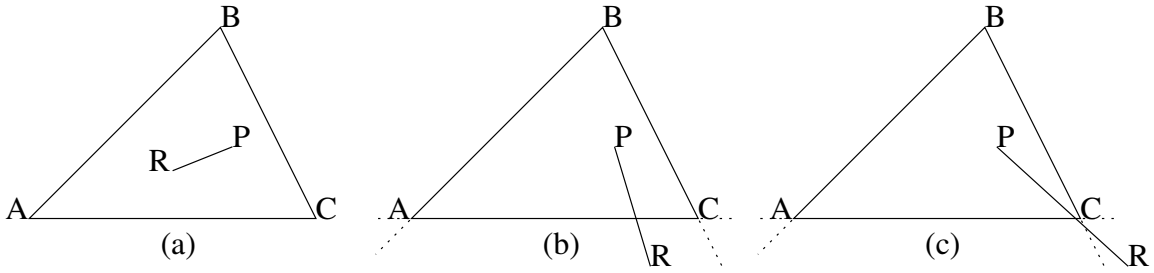

Figure 2.1: Arbitrary Reference Point R and a Random Point P in an Arbitrary Triangle $\triangle ABC$.

2.4.1 Arbitrary Triangles

Consider an arbitrary triangle $\triangle ABC$ with a random point P inside. The problem is to find the distribution of the distance between an arbitrary reference point R, and the random point P. Based on the location of R, we divide the problem into two sub-problems as below.

An Interior Reference Point

In Fig. 2.1(a), the reference point R is located inside an arbitrary triangle $\triangle ABC$. The random point P is also located inside the triangle. The problem is to find the distribution of the distances between R and any random point P.

An Exterior Reference Point

Figure 2.1(b) and (c) correspond to the case where the reference point R is located outside the triangle. In Fig. 2.1(c), the reference point R is located in the area formed from the extensions of the edges at vertex C, while in Fig. 2.1(b), the reference point is located outside of this specific area for any of the vertices. The two cases will be separately discussed.

2.4.2 Arbitrary Polygons

Using the decomposition and recursion scheme, we extend the proposed approach to deal with the distance distributions to arbitrary polygons. Note that for concave polygons, the distance denotes the shortest distance between two points. Thus, the line segment connecting two points in a concave polygon may be partly located outside of the polygon. Similar to the problem defined for arbitrary triangles, arbitrary interior

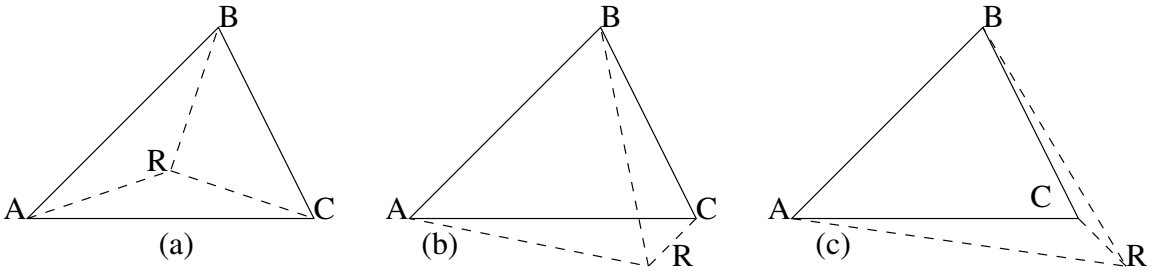

Figure 2.2: Decomposition.

and exterior reference points are considered for polygons as well. The approach and results are presented in Section 2.6.

2.5 Distance Distributions to Arbitrary Triangles

In this section, we describe how we employ decomposition and recursion to find the distance distributions from an arbitrary interior/exterior reference point to a random point within an arbitrary triangle. Specifically, according to the recursive approach, the problem is simplified to obtaining the distance distributions from the vertices of an arbitrary triangle. To solve this, similar to our previous work [54], the area-ratio approach is utilized.

2.5.1 Decomposition and Recursion

Here, we describe how the distance distributions from an arbitrary reference point to an arbitrary triangle can be obtained given that the distance distributions from the vertices are known. Later, we explain in detail how the distance distributions from the vertices can be obtained.

The Interior Reference Point

When the reference point R is located inside the triangle, connecting R to the vertices will decompose the triangle into three smaller triangles: $\triangle ABR$, $\triangle BCR$, and $\triangle ARC$, as shown in Fig. 2.2(a).

Assume that the distance distribution from a vertex of an arbitrary triangle to a random point within the triangle is known (will be explained in detail in Section 2.5.2). In other words, given $\triangle ABR$, the distance distribution from point R to a random point inside is known. Similarly, assume that the distance distributions

from R to a random point inside $\triangle BCR$ and $\triangle ARC$ are known as well. The Cumulative Distribution Function (CDF) of the distance from R to a random point within $\triangle ABC$ is the probabilistic sum of the distance distributions from R to a random point within the three triangles that constitute $\triangle ABC$. Denote the area of $\triangle ABC$, $\triangle ABR$, $\triangle BCR$, and $\triangle ARC$ as $||\triangle ABC||$, $||\triangle ABR||$, $||\triangle BCR||$, and $||\triangle ARC||$, respectively. Thus, according to the probabilistic sum

$$F_{ABC}(r) = \frac{||\triangle ABR||}{||\triangle ABC||}F_{ABR}(r) + \frac{||\triangle BCR||}{||\triangle ABC||}F_{BCR}(r) + \frac{||\triangle ARC||}{||\triangle ABC||}F_{ARC}(r), \quad (2.1)$$

where $F_t(r)$ corresponds to the CDF of the distance from point R to a random point inside triangle t, and r is the random variable representing the distance between R and a random point inside the triangle. Note that this probabilistic sum is based on the area ratio and it holds if the nodes are uniformly distributed at random in each area, which is the case in this dissertation.

The Exterior Reference Point

When R is located outside of $\triangle ABC$, two possible cases can happen as shown in Fig. 2.2(b) and (c): 1) the reference point is located in the area formed by the extensions of the edges at one vertex, as shown in Fig. 2.1(c) and Fig. 2.2(c), 2) the exterior reference point is at any location, but not the specific areas formed from the extension of the edges at the vertices, as shown in Fig. 2.1(b) and Fig. 2.2(b). As demonstrated in Fig. 2.2(c), connecting R to the vertices does not intersect with any of the edges, while in Fig. 2.2(b), connecting R to vertex B, intersects with edge AC, thus resulting in a different decomposition pattern.

As demonstrated in Fig. 2.2(b), using the probabilistic sum we have

$$\frac{||\triangle ABC||}{||\square ABCR||}F_{ABC}(r) + \frac{||\triangle ACR||}{||\square ABCR||}F_{ACR}(r) = \frac{||\triangle ABR||}{||\square ABCR||}F_{ABR}(r) + \frac{||\triangle BCR||}{||\square ABCR||}F_{BCR}(r), \quad (2.2)$$

where $||\square ABCR||$ is the area of the 4-gon $\square ABCR$. As a result, $F_{ABC}(r)$ can be obtained since all other terms in (2.2) are known (or can be obtained using the approach in Section 2.5.2).

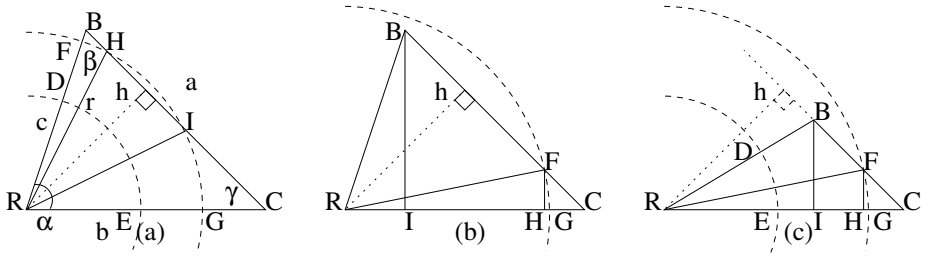

Figure 2.3: Distance Distributions from Vertex R to a Random Point Inside.

According to Fig. 2.2(c), we have

$$F_{ABR}(r) = \frac{||\triangle ABC||}{||\triangle ABR||} F_{ABC}(r) + \frac{||\triangle BRC||}{||\triangle ABR||} F_{BRC}(r) + \frac{||\triangle ACR||}{||\triangle ABR||} F_{ACR}(r). \quad (2.3)$$

Thus, $F_{ABC}(r)$ can be found given that all other terms are known.

2.5.2 Distance Distributions from a Vertex of an Arbitrary Triangle

As explained in the previous section, deriving the distance distributions from an arbitrary reference point R to a random point inside an arbitrary triangle is based on the distance distributions from the vertices of the triangle. In this section, we provide detailed explanation on how such distance distributions can be obtained. Consider $\triangle RBC$ where R is the reference point. Without loss of generality, assume that $|RB| \leq |RC|$. Two cases are separately discussed below.

The Inside Altitude Case

Figure 2.3(a) and (b) correspond to this case, where the perpendicular line from R to side BC is located inside $\triangle RBC$. In order to find the distance distribution from vertex R to a random point within $\triangle RBC$, based on the area-ratio approach, we start with drawing a disk centered at R, where the radius of the circle, denoted as r, corresponds to the distance between R and the random point within $\triangle RBC$. The probability that the distance is smaller than r, i.e., the corresponding CDF, is equal to the area of the intersection between the circle and $\triangle RBC$ divided by $||\triangle RBC||$. Four possible cases are discussed below, where h is the height from R to side BC and can be derived as

$$h = \frac{2||\triangle RBC||}{|BC|}, \quad (2.4)$$

where

$$||\triangle RBC|| = \sqrt{s(s-|RB|)(s-|BC|)(s-|RC|)}, \tag{2.5}$$

and

$$s = \frac{|RB|+|BC|+|RC|}{2}. \tag{2.6}$$

i. $0 \leq r \leq h$

As shown in Fig. 2.3(a), the disk with radius r intersects the triangle at two points D and E. The intersection area between the disk and the triangle can be easily calculated as $\frac{\alpha}{2}r^2$, where α is $\angle BRC$.

ii. $h \leq r \leq |RB|$

As demonstrated in Fig. 2.3(a), the disk with radius $h \leq r \leq |RB|$ cuts side BC at two points H and I, side RB at F, and side RC at G. The intersection area can be found as $|| \lhd RFH|| + ||\triangle RHI|| + || \lhd RIG||$. The area of $\triangle RHI$ is $\frac{h|HI|}{2}$, where the length of HI is

$$|HI| = 2\sqrt{r^2-h^2}. \tag{2.7}$$

Let us denote the angle $\angle HRI$ as α_1. The sum of the areas of $\lhd RFH$ and $\lhd RIG$ can be calculated as the sector with radius $\alpha - \alpha_1$, where

$$\frac{\alpha_1}{2} = \cos^{-1}\left(\frac{h}{r}\right). \tag{2.8}$$

Thus,

$$|| \lhd RFH|| + || \lhd RIG|| = \frac{\alpha-\alpha_1}{2}r^2. \tag{2.9}$$

iii. $|RB| \leq r \leq |RC|$

The intersection area can be calculated as $||\triangle RBF|| + || \lhd RFG||$, as demonstrated in Fig. 2.3(b). $||\triangle RBF||$ can be expressed as $\frac{h|BF|}{2}$, where

$$|BF| = \sqrt{|RB|^2-h^2} + \sqrt{r^2-h^2}. \tag{2.10}$$

$|| \lhd RFG||$, which is the area of a sector of the disk can be calculated as $\frac{\alpha_2}{2}r^2$, in which

$$\alpha_2 = \alpha - \left(\cos^{-1}\left(\frac{h}{|RB|}\right) + \cos^{-1}\left(\frac{h}{r}\right)\right). \tag{2.11}$$

iv. $r \geq |RC|$

When $r \geq |RC|$, the disk with radius r will cover the entire triangle. Thus, the intersection area is equal to the area of $\triangle RBC$.

The Outside Altitude Case

As shown in Fig. 2.3(c), the perpendicular line from R to side BC falls outside of $\triangle RBC$. Three cases are discussed below.

i. $0 \leq r \leq |RB|$

The disk with radius r and centered at R, intersects $\triangle RBC$ at two points D and E. The intersection area, i.e., the area of sector $\triangleleft RDE$, can be easily calculated as $\frac{\alpha}{2}r^2$, where α is $\angle BRC$ of the triangle $\triangle RBC$ and is known.

ii. $|RB| \leq r \leq |RC|$

The intersection area consists of two parts: the area of $\triangle RBF$ plus the area of $\triangleleft RFG$. The area of $\triangle RBF$ is

$$||\triangle RBF|| = \frac{h|BF|}{2}, \tag{2.12}$$

where, $|BF| = \sqrt{r^2 - h^2} - \sqrt{|RB|^2 - h^2}$.

Finally, the area of sector $\triangleleft RFG$ is

$$|| \triangleleft RFG|| = \frac{\sin^{-1}\left(\frac{h}{r}\right) - \gamma}{2} r^2, \tag{2.13}$$

where γ is the angle $\angle BCR$ shown in Fig. 2.3(a).

iii. $r \geq |RC|$

When $r \geq |RC|$, the triangle will be completely inside of the disk with radius r. Thus, the intersection area is equal to the area of $\triangle RBC$.

Algorithm 1 demonstrates the process of obtaining the distance distributions from an arbitrary reference point to an arbitrary triangle based on the location of the reference point, the distance distributions from the vertices of the triangle, and the probabilistic sum. The **vertex** method, returns the distance distributions from vertex

Algorithm 1 Distance Distribution from an Arbitrary Reference Point R to an Arbitrary Triangle $\triangle ABC$

if R is the same as one of the vertices (say C) **then**
  $F(r)$ = **vertex**(A,B,R)
end if
if R is an interior reference point **then**
  $F_1(r)$ = **vertex**(A,B,R)
  $F_2(r)$ = **vertex**(A,C,R)
  $F_3(r)$ = **vertex**(B,C,R)
  $F(r)$ = **p-sum**($F_1(r)$,$F_2(r)$,$F_3(r)$)
end if
if R is an exterior reference point **then**
  if R is outside of the areas formed by the extensions of the edges (say R is near to side AC) **then**
    $F_1(r)$ = **vertex**(A,B,R)
    $F_2(r)$ = **vertex**(B,C,R)
    $F_3(r)$ = **vertex**(A,C,R)
    $F(r)$ = **p-sum**($F_1(r)$,$F_2(r)$,$-F_3(r)$)
  else /*R is within the area formed from the extensions of the edges of a vertex (say vertex C)*/
    $F_1(r)$ = **vertex**(A,B,R)
    $F_2(r)$ = **vertex**(B,C,R)
    $F_3(r)$ = **vertex**(A,C,R)
    $F(r)$ = **p-sum**($F_1(r)$,$-F_2(r)$,$-F_3(r)$)
  end if
end if

R of a triangle. If h (the perpendicular line from R to side BC) is inside $\triangle BCR$, **vertex**(B,C,R) will return the following

$$\frac{1}{||BCR||}\begin{cases} \frac{\alpha}{2}r^2 & 0 \le r \le h \\ \frac{2h\sqrt{r^2-h^2}}{2} + \frac{\alpha-\alpha_1}{2}r^2 & h \le r \le |RB| \\ \frac{h\left(\sqrt{|RB|^2-h^2}+\sqrt{r^2-h^2}\right)}{2} + \frac{\alpha_2}{2}r^2 & |RB| \le r \le |RC| \\ ||BCR|| & r \ge |RC| \end{cases}. \tag{2.14}$$

If h is outside of the triangle, **vertex**(B,C,R) will return

$$\frac{1}{||BCR||}\begin{cases} \frac{\alpha}{2}r^2 & 0 \le r \le RB \\ \frac{h\left(\sqrt{r^2-h^2}-\sqrt{|RB|^2-h^2}\right)}{2} + \frac{\sin^{-1}\left(\frac{h}{r}\right)-\gamma}{2}r^2 & h \le r \le |RB| \\ ||BCR|| & r \ge |RC| \end{cases}. \tag{2.15}$$

The **p-sum**($F_1(r)$,$F_2(r)$,$F_3(r)$) method, returns the probabilistic sum of $F_1(r)$, $F_2(r)$, and $F_3(r)$.

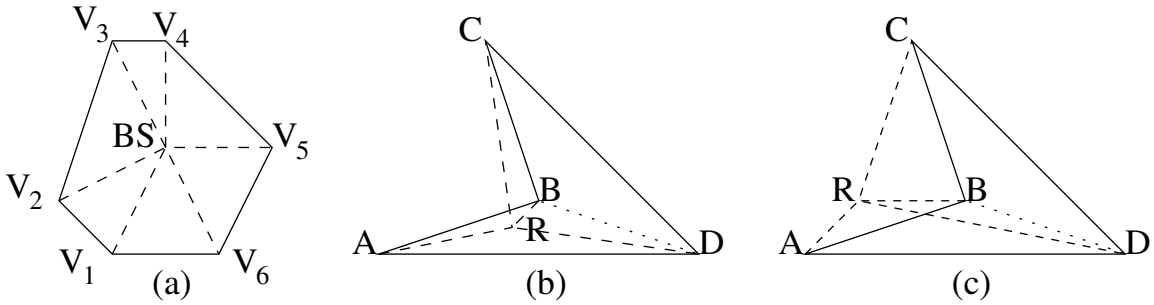

Figure 2.4: Triangulation of Convex/Concave Polygons.

2.6 Random Distances to Arbitrary Polygons

As shown in Fig. 2.4, any convex or concave polygon can be triangulated and thus our approach can be applied. In Fig. 2.4(a), the distance distribution from the BS to a random point within the cell, in the shape of an irregular convex polygon, can be found by using the probabilistic sum of the distance distributions between the BS and a random point in each of the triangles. Specifically, for each of the triangles, the distance distribution from the vertex, i.e., the BS, should be obtained as explained in Section 2.5.2.

In Fig. 2.4(b), $\square ABCD$, which is an irregular concave polygon, is decomposed into $\triangle ABD$ and $\triangle BCD$. The distance distribution from an interior R to a random point inside $\square ABCD$ can be obtained by the probabilistic sum of the distance distributions from R as an interior reference point to $\triangle ABD$ and as an exterior reference point to $\triangle BCD$ using the approach explained in Section 2.5.

Finally, in Fig. 2.4(c), the distance distribution from an exterior R to a random point inside $\square ABCD$, an irregular concave polygon, can be obtained by the probabilistic sum of the distance distributions from R as an exterior reference point to $\triangle ABD$ and $\triangle BCD$. Thus, our approach can be applied to convex/concave polygons with an interior/exterior reference point.

2.7 Results and Verification of the Distance Distributions to Arbitrary Triangles and Polygons

In this section, we first provide two examples to obtain the distance distributions from an arbitrary interior/exterior reference point to a random point within an arbitrary triangle. Then, we give two examples to verify our results for arbitrary polygons with

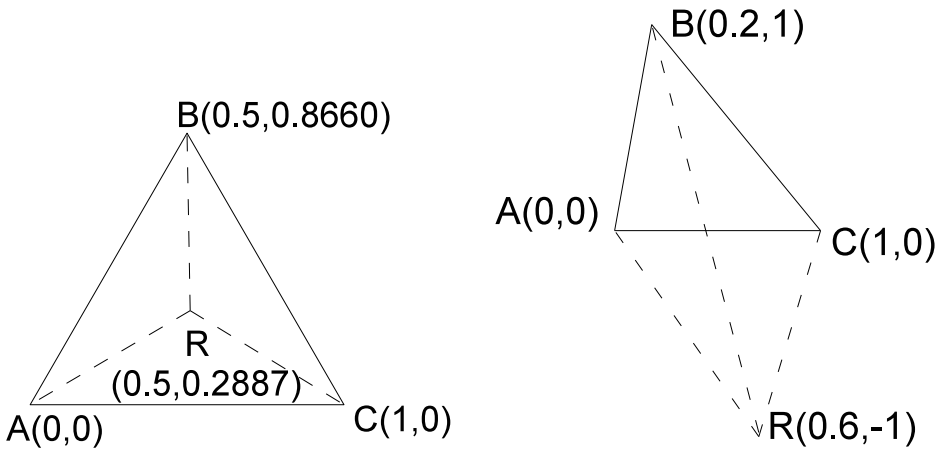

(a) An Interior Reference Point (b) An Exterior Reference Point

Figure 2.5: An Arbitrary Triangle with an Interior/Exterior Reference Point

arbitrary interior and exterior reference points. We compare our results with those of simulation and with the results from existing work where applicable. All simulations, analytical derivations, and numerical results are done in Matlab.

2.7.1 Example 1: An Equilateral Triangle with an Interior Reference Point

Denote the vertices of the triangle, A, B, and C with coordinates $(0,0)$, $(\frac{1}{2}, \frac{\sqrt{3}}{2})$, and $(1,0)$, respectively, assuming that A is the origin. Moreover, assume that R is located at the geometrical center of the triangle, $(\frac{1}{2}, \frac{\sqrt{3}}{6})$. As shown in Fig. 2.5(a), connecting R to the vertices of $\triangle ABC$ decomposes the triangle into three triangles: $\triangle ARC$, $\triangle ABR$, and $\triangle BCR$. As explained earlier in Section 2.5.1, using the recursive approach we have

$$F_{ABC}(r) = \frac{1}{3}F_{ARC}(r) + \frac{1}{3}F_{ABR}(r) + \frac{1}{3}F_{BCR}(r), \tag{2.16}$$

where the area of the three small triangles is the same and is equal to $\frac{1}{3}||\triangle ABC||$, and F denotes the CDF.

Based on the approach explained in Section 2.5.2, we obtain that $F_{ARC}(r) = F_{ABR}(r) = F_{BCR}(r)$, and is equal to

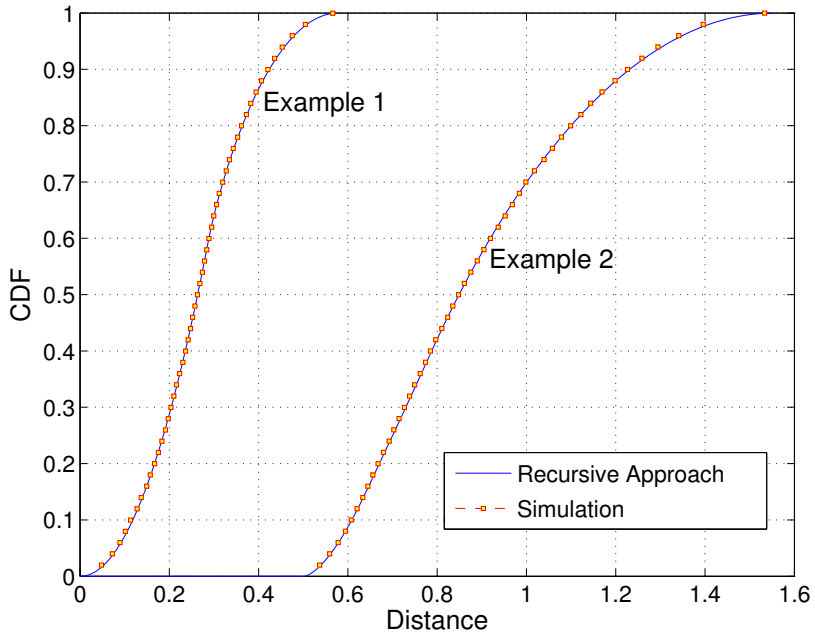

Figure 2.6: Recursive Approach vs. Simulation: Example 1 (An Interior Reference Point) in Section 2.7.1 and Example 2 (An Exterior Reference Point) in Section 2.7.2.

$$\begin{cases} \frac{4}{3}\pi\sqrt{3}r^2 & 0 \le r \le \frac{\sqrt{3}}{6} \\ 2\sqrt{r^2-\frac{1}{12}} - 4\sqrt{3}r^2\cos^{-1}\frac{\sqrt{3}}{6r} & \\ \quad + \frac{4}{3}\pi\sqrt{3}r^2 & \frac{\sqrt{3}}{6} \le r \le \frac{\sqrt{3}}{2} - \frac{\sqrt{3}}{6} \\ 1 & r \ge \frac{\sqrt{3}}{2} - \frac{\sqrt{3}}{6} \end{cases}. \tag{2.17}$$

Then, based on (2.16) and (2.17), $F_{ABC}(r)$ can be obtained, which is equal to (2.17). Since $\triangle ABC$ is an equilateral triangle and R is an interior reference point, the approach in [31] applies as well. The mathematical expressions obtained by our approach precisely match with the expressions provided by the Matlab code of [31], verifying our approach and results.

Finally, we compare the above results with the numerical results from simulation. At each run, a node is randomly generated inside the triangle and the distance between R and the random point is measured. The experiment was done for $20,000$ times and the CDF was drawn. As shown in Fig. 2.6, the results from our recursive approach match very closely with the simulation results. While our approach is very simple and easy to follow, it obtains accurate closed-form expressions.

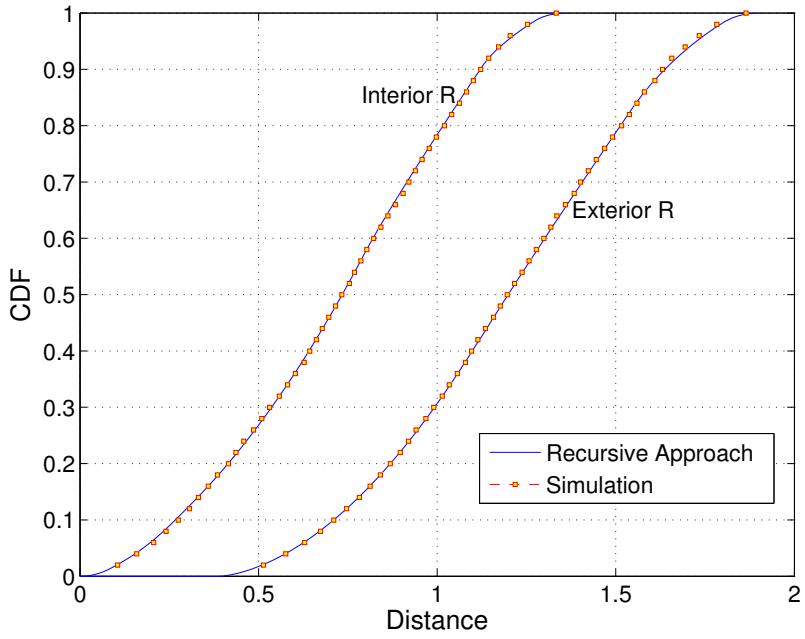

Figure 2.7: Comparing Results from Simulation and the Recursive Approach for an Arbitrary Polygon.

2.7.2 Example 2: An Arbitrary Triangle with an Exterior Reference Point

In this example, we investigate the case where R is located outside the triangle. The vertices of an arbitrary triangle are assumed to be $A(0,0)$, $B(0.2,1)$, and $C(1,0)$, with A as the origin, as shown in Fig. 2.5(b). The reference point R is located at $(0.6,-1)$.

Based on the probabilistic sum we have

$$\frac{||\triangle ABR||}{||\square ABCR||}F_{ABR}(r)+\frac{||\triangle BCR||}{||\square ABCR||}F_{BCR}(r)= \frac{||\triangle ABC||}{||\square ABCR||}F_{ABC}(r)+\frac{||\triangle ACR||}{||\square ABCR||}F_{ACR}(r). \tag{2.18}$$

$F_{ABR}(r)$, $F_{BCR}(r)$, and $F_{ACR}(r)$ can be derived noting that they correspond to the distance distributions from a vertex of a triangle. Finally, $F_{ABC}(r)$ can be obtained based on (2.18).

Since no existing work is available for obtaining the distance distributions from an exterior arbitrary reference point to an arbitrary triangle, we compare our results

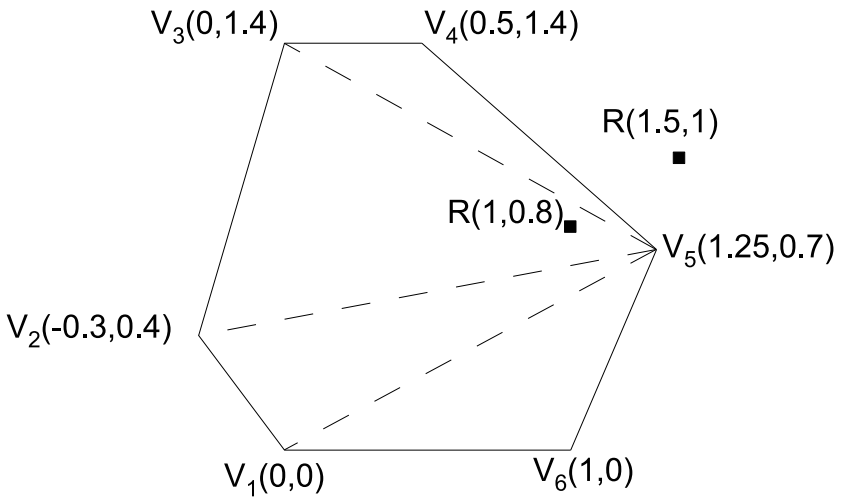

Figure 2.8: An Arbitrary Polygon with an Arbitrary Interior/Exterior Reference Point. Different triangulations will still lead to the same results.

only with those of simulations. Figure 2.6 demonstrates this comparison. As shown in the figure, the results match closely, verifying our approach and results.

2.7.3 Verification of the Results for Arbitrary Polygons

To demonstrate and verify our approach and results for arbitrary polygons, we present two examples with arbitrary interior and exterior reference points. First, consider an arbitrary polygon as shown in Fig. 2.8 with an arbitrary interior reference point R located at $(1, 0.8)$. The vertices of the polygon are $V_1(0, 0)$, $V_2(-0.3, 0.4)$, $V_3(0, 1.4)$, $V_4(0.5, 1.4)$, $V_5(1.25, 0.7)$, and $V_6(1, 0)$. As demonstrated in the figure, the polygon can be triangulated into 4 triangles $\triangle V_1V_2V_5$, $\triangle V_2V_3V_5$, $\triangle V_3V_4V_5$, and $\triangle V_1V_5V_6$. The distribution of the distance from R to the polygon is the probabilistic sum of the distance distribution from R to $\triangle V_1V_2V_5$, $\triangle V_3V_4V_5$, and $\triangle V_1V_5V_6$, as an exterior reference point, and to $\triangle V_2V_3V_5$ as an interior reference point. Figure 2.7 shows the results from the simulation and those from our proposed recursive approach. It is observed that the results match closely which verifies the correctness of our obtained analytical results.

Furthermore, consider the same arbitrary polygon in Fig. 2.8 with R located at $(1.5, 1)$, as an exterior reference point. The distance distribution from R to the polygon is the probabilistic sum of the distance distributions from R, as an exterior reference point, to the four triangles that constitute the polygon. The CDF of the

distance between R and a random point inside the polygon is shown in Fig. 2.7 and is compared with simulation results, where a good match can be observed.

2.8 Applications in Wireless Communication Networks

In this section, through case studies, we demonstrate how the distance distributions obtained in this chapter are used to address important networking research problems. In the next chapter, we will show in detail how the approach and results from this chapter are used for interference analysis in a femto cognitive radio network. In this section, however, we will demonstrate the application of our results in general wireless communications research problems.

First, we investigate the distribution of the k-th nearest neighbor (including the nearest and farthest) from a given reference point. Specifically, choosing the nearest neighbor in a sparse network and the farthest reachable neighbor in a dense network can reduce the energy consumption and routing overhead, respectively [57]. This can be important in designing routing algorithms for a cognitive radio network or any other kind of network. Thus, it is useful to characterize the distribution of the k-th nearest neighbor of a specific node in a wireless network.

Second, using the approach presented in this chapter, the distribution of the distance in a tiered or hierarchical network with an arbitrary polygon-shaped cell is derived. These distance distributions are extremely helpful in the modeling and analysis of tiered/heterogeneous cognitive networks, such as networks consisting of macro and femto cells. In the next chapter, we will show how such distance distributions are used for performance evaluation of a heterogeneous network consisting of macro/femto cells in terms of the SIR and outage probability.

2.8.1 k-th Nearest Neighbor

Utilizing the distance distributions from a given reference point R, as proposed in this chapter, based on order statistics, the distribution of the distance from R to its k-th nearest neighbor can be obtained as below [43]

$$f_k(r) = (1 - F(r))^{N-k} F(r)^{k-1} f(r) \frac{(N)!}{(N-k)!(k-1)!}, \tag{2.19}$$

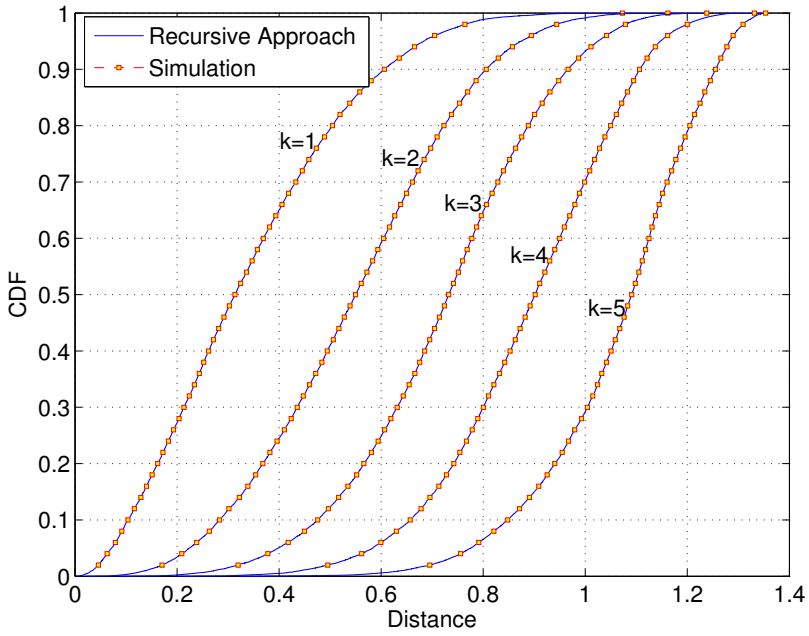

Figure 2.9: k-th Nearest Neighbor (R located at $(1, 0.8)$).

where $f_k(r)$ denotes the distance distribution of the k-th nearest neighbor of node R, $F(r)$ and $f(r)$ are the CDF and PDF of the distance from the reference point R, respectively, and N is the number of nodes in the cell (excluding R).

Here, we investigate the distribution of the k-th nearest neighbor from R in a case study. Consider the cell setting demonstrated in Fig. 2.8, where R is an arbitrary interior reference point located at $(1, 0.8)$. In a real scenario, R could be one of the random nodes deployed within the cell with any location. The number of nodes N is assumed to be 5. In Section 2.6, we explained in detail how the CDF of the distance (denoted as $F(r)$) from R to a random point within the polygon can be obtained. Obviously,

$$f(r) = (F(r))'. \tag{2.20}$$

Given $f(r)$ and $F(r)$, the PDF of the distance to the k-th nearest neighbor can be obtained according to (2.19). Figure 2.9 demonstrates the distance CDF of the k-th nearest neighbor from simulation and the recursive approach presented in this chapter. As demonstrated in the figure, the analytical and simulation results demonstrate a

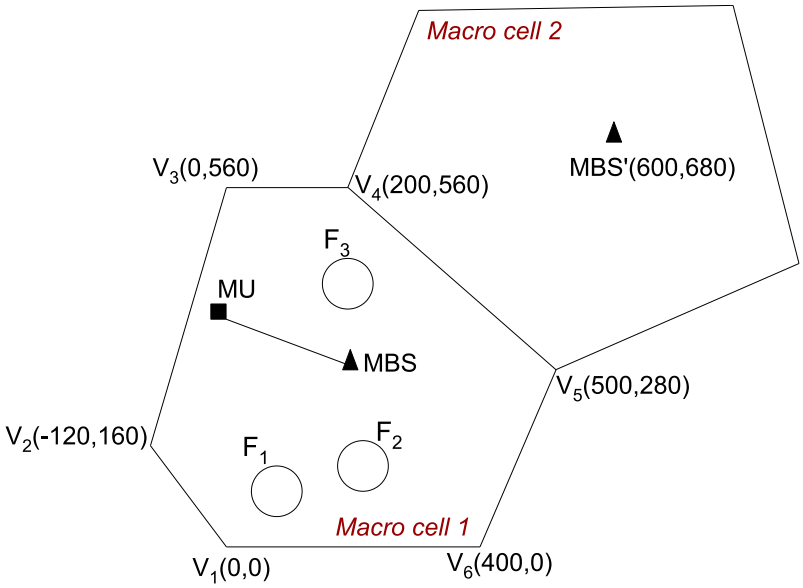

Figure 2.10: A Heterogeneous Network: MU is Located in the Macro Cell but Outside of all Femto Cells.

very close match which can verify the accuracy of our approach. Note that the CDF curves labeled as $k = 1$ and $k = 5$ correspond to the nearest and farthest neighbors of R, respectively.

2.8.2 MBS-MU Distance Distribution in A Tiered/Hierarchical Network

As another practical scenario, consider a heterogeneous network consisting of a single macro cell and multiple cognitive femto cells, as shown in Fig. 2.10. As demonstrated in the figure, the coverage area of the macro cell is assumed to be an irregular polygon. For ease of presentation and without loss of generality, the coverage area of each cognitive femto cell is approximated by a disk with radius 40 m [22]. The Macro Base Station (MBS) is located at $(200, 280)$, where the origin is at $\mathrm{V}_1(0, 0)$. There are three femto cells with centers at $F_1(80, 80)$, $F_2(240, 120)$, and $F_3(200, 400)$.

Assume that the cellular users that are outside the coverage area of all femto cells are denoted as Macro Users (MUs) which communicate with the MBS. We call this structure a tiered or hierarchical structure in which the MUs are not uniformly distributed within the polygon area representing the macro cell.

Let $F_H(h)$ denote the CDF of the distance from a random node within the macro

cell to the MBS. Also, let $F_{C_i}(c_i)$ be the CDF of the distance from the MBS to a random point within femto cell i, for all i. Finally, $F_X(x)$ denotes the distribution of the distance from the MBS to the MU. Then, according to the probabilistic sum

$$F_H(h) = \frac{A - \sum_i a_i}{A} F_X(x) + \sum_i \frac{a_i}{A} F_{C_i}(c_i), \tag{2.21}$$

where A is the area of the macro cell and a_i is that of femto cell i. Note that $F_H(h)$ can be obtained based on the decomposition and recursion approach explained in Section 2.5 and Section 2.6. Further, $F_{C_i}(c_i)$ is the distance distribution from an exterior reference point to a random point inside disk i, which can be easily obtained. Thus, according to (2.21), $F_X(x)$ can be obtained. Note that the coverage area of the femto cells is not confined to being a disk and could be any arbitrary polygon.

As a case study, for the scenario shown in Fig. 2.10, the CDF of the distance from the MBS to a random MU is obtained and compared with the simulation results. Figure 2.11 shows a close match between the analytical and simulation results.

Given the distribution of d as above, the distribution of the received signal can be obtained. Similarly, the distribution of the interference in a given network can be found. Then, important performance metrics such as the SIR and outage probability can be derived. Please refer to the next chapter for further details.

2.8.3 Other-Cell MBS-MU Distance Distribution in A Tiered/Hierarchical Network

In this scenario, we extend the previous case study and investigate the distribution of the distance from an MU to other-cell MBS, where the cell containing the MU is in the shape of an irregular polygon. With our results, for the first time in the literature, other-cell interference analysis for arbitrarily polygon-shaped finite networks becomes possible.

The same equation in (2.21), with different notation, can be used to obtain the distribution of the distance, denoted as $F_X(x)$, between an external MBS (MBS′) to an MU in another macro cell. Referring to (2.21), here, $F_H(h)$ denotes the distance distribution from MBS' to a random node in the irregular-shaped macro cell 1, which can only be derived using the approach proposed in this paper. $F_{C_i}(c_i)$ denotes the distribution of the distance from MBS′ to femto cell i, which can be easily obtained given that the femto cells are approximated with disks. If femto cells are approximated

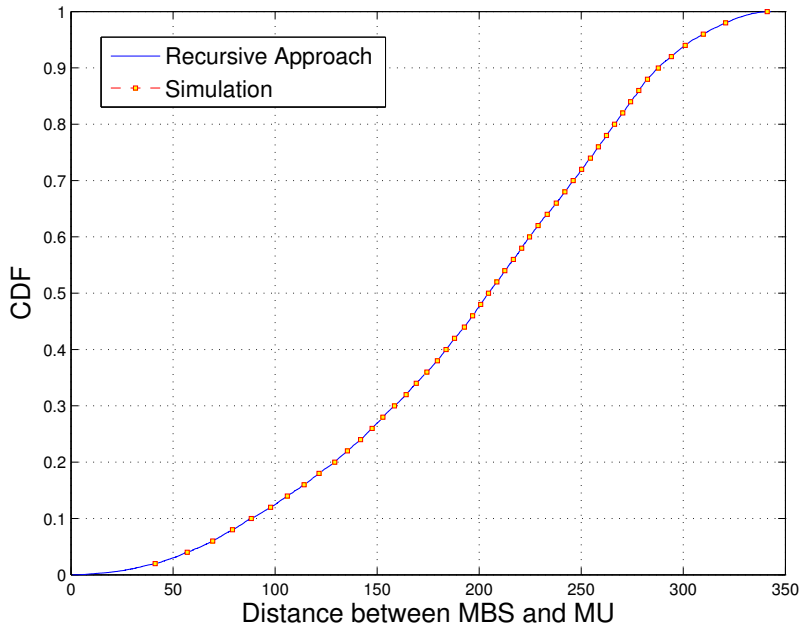

Figure 2.11: CDF of the Distance between the MBS and a Random MU, where the Macro Cell is an Arbitrary Polygon.

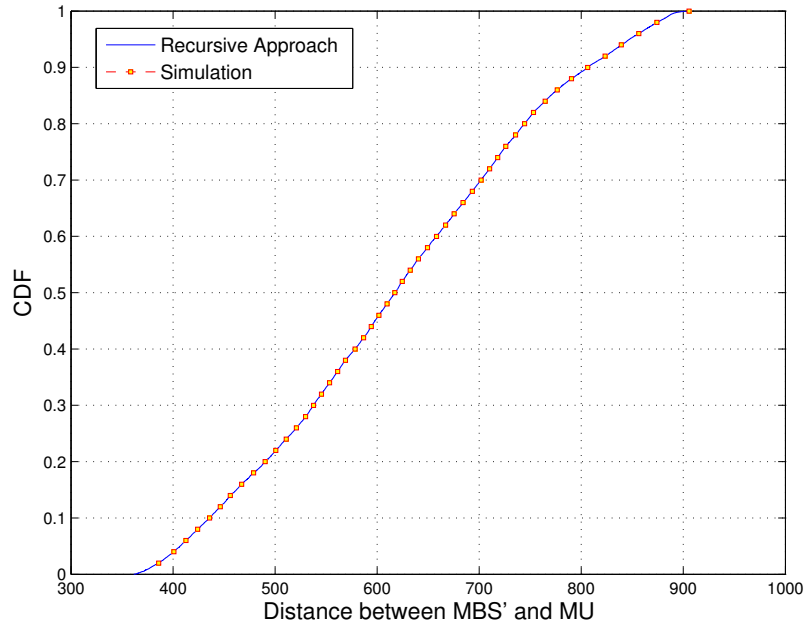

Figure 2.12: CDF of the Distance between an Other-Cell MBS and a Random MU, where the Macro Cell is an Arbitrary Polygon.

with irregular polygons, the approach explained in this paper shall be used to obtain the corresponding distributions.

Consider the scenario shown in Fig. 2.10, in which the other-cell MBS is located at $(600, 680)$ and the FUs are randomly distributed in disk-shaped femto cells with centers at $F_1(80, 80)$, $F_2(240, 120)$, and $F_3(200, 400)$ and a radius of 40 m. The MU is randomly distributed in macro cell 1, but outside all femto cells. Figure 2.12 shows the results, for the CDF of the distance between an MU and an other-cell MBS, from our recursive approach compared with the simulations, where a close match is observed.

2.9 Conclusions

Motivated by the importance of interference in the design and analysis of cognitive radio networks and according to the fact that the interference is a function of the distance between the nodes, in this chapter, we focused on the problem of obtaining distance distributions from an arbitrary reference point to an arbitrary polygon.

We proposed a systematic approach based on decomposition and recursion to find the distance distributions from an arbitrary reference point to a random point within an arbitrary polygon. The reference point can be located inside or outside of the polygon, and the polygon can be any arbitrary convex/concave polygon. Furthermore, through case studies, we showed the application of our scheme and results in wireless communication-related research problems.

Having the distance distributions from a given reference point to a random point within a polygon can greatly help with the analysis of wireless networks, where, in real-world, the shapes of the cells are irregular. Using these distance distributions, the distributions of the distance-related metrics, such as interference, can be derived. In the next chapter, we discuss how the distance distributions derived in this chapter are utilized to analyze the cumulative interference in a cognitive radio network scenario.

Chapter 3

Performance Analysis for a Heterogeneous Cognitive Radio Network

3.1 Overview

In Chapters 1 and 2, we discussed the importance of the interference analysis on the design and analysis of spectrum allocation schemes for cognitive radio networks. In this chapter, we consider a cellular network consisting of a macro cell and multiple cognitive femto cells (small cells). Using the distance distributions derived in the previous chapter, we obtain the distribution of the interference and signal-to-interference ratio. Having the distribution of the SIR, we can investigate important performance metrics such as the outage probability. Detailed numerical and simulation results on the cumulative interference and SIR are given to illustrate the accuracy of our analysis using the node distance distributions obtained in Chapter 2, and to shed light on the performance analysis of a two-tier cellular network with cognitive femto cells. Parts of the work presented in this Chapter has been published previously [10].

3.2 Introduction

It is predicted that the global mobile data traffic will increase almost 10 times between 2014 and 2019, and the mobile network connection speeds will increase more than twice by 2019 [1].

Based on the observed facts and predictions, researchers from academia along with industry partners have been working on finding solutions that can handle the huge demand of data traffic in the near future. To catch up with the demand, the aggregate data rate will need to increase by approximately 1000x from 4G to 5G [13]. The aggregate data rate refers to the total amount of data that the network can serve. Furthermore, it is predicted that a single macro cell may need to support over 10,000 low-rate devices plus its traditional high-rate mobile users [13].

One of the key technologies in 5G that will help with obtaining the 1000-fold data rate is extreme densification [13]. Extreme densification and offloading lead to improved spectral efficiency and more active nodes per unit area. Small (femto) cells have been introduced as the solution to reach extreme densification.

From another point of view, a large amount of data traffic, according to [29], is originated from indoor environments (e.g., homes, offices, and shopping malls). In the near future, about 60% of voice and 90% of data will originate from indoor environments, where the cellular network quality is known to be poor due to the penetration loss of signal between indoor and outdoor environments. The dense deployment of base stations may seem as a solution to improve the cellular service quality in indoor environments, however, deploying more macro BSs can result in severe interference between the cells as these BSs usually transmit with a high power and cover large areas. Moreover, the deployment cost of cellular BSs as well as their power consumption and maintenance cost is very high, which makes the dense deployment of cellular BSs not practical and cost-effective.

Small cells have emerged as a solution to provide cellular services in indoor environments and dead zones, in order to improve the capacity of traditional cellular networks. Networks consisting of macro BSs and small cells are also referred to as tiered networks. Macro BSs (MBSs), which are the traditional cellular BSs, are usually deployed according to a priori planning and thus are regularly distributed (e.g., roughly based on hexagonal grids). On the other hand, femto cells are deployed within indoor environments or the places with poor cellular coverage, and their locations are considered to be random [21, 30]. Unlike macro BSs, Femto BSs (FBSs) use lower transmission powers and cover smaller areas. They provide better cellular services for indoor users, while their deployment and maintenance cost is lower. Moreover, because of their low transmission powers and short-range communications, they can coexist with macro BSs and transmit at the same time.

Despite the benefits of deploying femto cells that improve the network capacity

and user experience, they can possibly impose harmful interference on the macro cell transmissions if the femto cells are deployed on a large scale. As a result, accurate analysis of the interference from femto cells to macro cells, and vice versa, is of great importance. This interference analysis can provide us with deep insights into important performance metrics, such as the SIR, network capacity, outage probability, etc.

In existing literature, stochastic geometry has been used for interference analysis in tiered networks. However, the existing work based on stochastic geometry assumed that the macro and femto BSs are deployed randomly according to a PPP [16,30,42], which is not a realistic assumption. At least for the macro BSs, they are deployed according to cell planning and their locations are not random. Moreover, stochastic geometry provides us with average results over time and space, but cannot present performance results for a specific network deployment and/or a time instance. Furthermore, many realistic networks consist of a finite number of users and BSs located within a finite region. However, stochastic geometry usually provides insights into performance results for a "typical user" over an infinite region, independent of the location of the user, which is not accurate for finite networks, as the signal power and interference attenuate with distance and thus the location of the users can greatly affect the network performance. In finite networks, performance results directly depend on the shape of the cell and the location of users. According to the facts explained above and unlike stochastic geometry, we propose an approach that is capable of investigating the performance of a finite-region network with a finite number of nodes, where the locations of some of the nodes are determined in advance.

In this chapter, using the scheme and results regarding the node distance distributions obtained in the previous chapter, we obtain the distributions of the signal, interference, and SIR for both macro and femto cells, focusing on an uplink resource reusing scenario. The obtained results are further utilized to quantify the system performance, such as the outage probability. Unlike the stochastic geometry tool, with the proposed model, the network performance metrics for a specific network deployment, a specific user, and/or time instance are able to be accurately analyzed. Specifically, according to the general path-loss model commonly used in wireless communication networks, the signal and interference at a receiving node from a transmitting/interfering node depend heavily on the distance between them. To model and analyze the signal and interference at a macro/femto BS in the uplink scenario, we first obtain the distribution of the distance between a given reference node (e.g., MBS

or FBS) and a randomly-located cellular user for both macro and femto cells, without having any limitations on the shapes of the cells or the locations of the nodes. It is worth noting that the macro users are uniformly distributed conditioning on that the area of the femto cells are excluded.

The main contributions of this chapter are twofold. First, the approach proposed in Chapter 2 is extended to apply to the node distance distributions associated with arbitrarily-shaped cells in tiered cellular systems. The approach has no limitations on the location of the reference node (macro/femto BS). Therefore, an arbitrary deployment of femto cells within the macro cell is allowed. On the other hand, as will be discussed in Section 3.5, the approach can be easily extended to a system with nonuniformly-distributed users. Second, with the obtained distance distributions, we accurately model and analyze a cellular network consisting of multiple macro cells and randomly-deployed femto cells in the uplink resource reusing scenario. The distributions of signal, interference, and SIR are derived, based on which the system outage probability is obtained. The results presented in this work can provide us with fruitful insights into the performance metrics for femto and macro cells and can be used by the femto BSs and users to adjust their transmission powers to coexist with the macro BSs and users, and guarantee a specific outage probability for macro/femto cells.

3.3 Related Work

In various existing work [15,16,22,23,30], stochastic geometry was utilized to develop analytical frameworks for tiered heterogeneous networks, where femto cells are deployed based on a spatial process. In [30], considering a k-tiered network where the locations of the BSs follow a PPP, a stochastic geometry framework was developed to analyze the downlink SINR for a user. The outage probability was then obtained based on the CDF of the SINR. The biased user association was employed in which users choose tier-k BSs according to the maximum long-term averaged received power with bias. In [16], stochastic geometry was employed to derive the closed-form expressions for average downlink data rates. Similarly, with the biased cell association strategy, the authors took the spectrum allocation into consideration to jointly optimize the user association and spectrum allocation among tiers.

Cognitive femto cells were introduced as a promising technology for interference mitigation in tiered heterogeneous networks [21, 24]. Femto BSs with cognitive abili-

ties can obtain information about the transmissions in the macro cell and other femto cells. Thus, taking the interference into account, they can perform concurrent transmissions while satisfying a specific outage probability for every tier of the network. In [21], using a stochastic geometry model, the bounds on the maximum intensity of simultaneously active femto cells were obtained based on the fact that the femto BSs are deployed according to a PPP. In [24], stochastic geometry was adopted to model and analyze a heterogeneous network with cognitive femto BSs, which are capable of sensing the spectrum and thus avoiding interference to the macro cell transmissions.

Recently, node distance distributions have been more increasingly used for the performance analysis of wireless networks. In [6], distance distributions associated with regular hexagons were used to obtain the distribution of the total interference on a specific BS from its neighboring transmitters. In [27], distance distributions associated with arbitrary shapes were utilized to propose a general framework for analytically obtaining the outage probability in finite networks. However, the results are not applicable when the intended reference point is located outside of the network cell.

Different from the existing work, we utilize distance distributions to accurately model and analyze a tiered heterogeneous network. Complementary to the results using stochastic geometry, our approach provides accurate performance analysis for a tiered network with arbitrarily-located macro/femto BSs and randomly-located users, without assuming an infinite network. Furthermore, the locations of macro/femto BSs do not have to follow a PPP. The results provided in our work based on the probabilistic distance models can be utilized by the cognitive femto cells to avoid harmful interference on the macro cells or other co-existing femto cells.

3.4 System Model

The two-tier system model considered in this chapter consists of a macro cell containing no less than one femto cell, where the cellular (macro) users are distributed uniformly at random within the macro cell except regions covered by femto cells. For ease of presentation, we first focus on the single macro cell model, however, in Section 3.6, we show in detail how our approach applies to multi macro cell scenarios. To demonstrate the applicability of our approach, we assume that the macro and femto cells have arbitrary irregular shapes. The BSs located in the macro and femto cells are denoted as MBS and FBS, respectively.

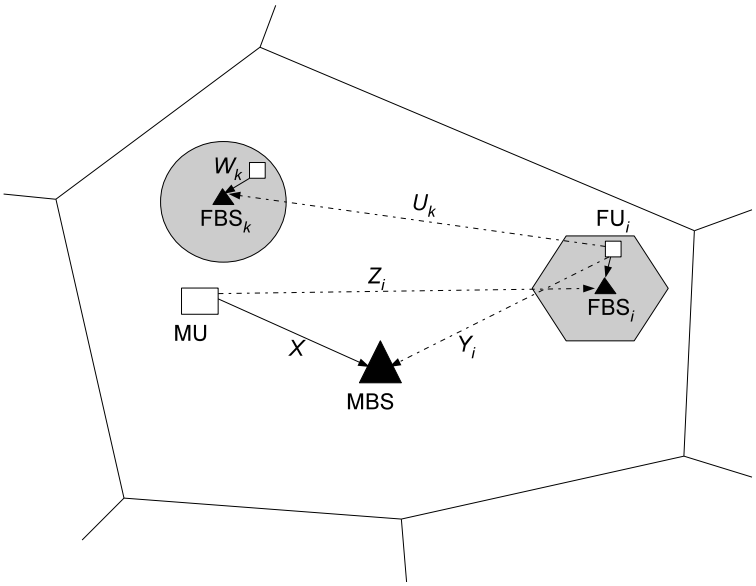

Figure 3.1: System model consisting of a macro cell and several femto cells in an uplink resource reusing scenario, where the solid arrow lines show the transmission from a user to its associated BS, and the dashed arrow lines show the interference at the BS from a user in other cell.

The cellular users communicate the BS in either uplink or downlink mode. In the uplink mode, the transmission happens from a user to the BS, while the direction is reversed in the downlink mode. We focus on the uplink scenario where in each cell, only one user is active at a time. For the downlink scenario, the applicability of our approach is discussed in Section 3.5.

A cellular user within the coverage area of an FBS will be associated to the corresponding femto cell and be identified as a Femto User (FU) with transmission power P_F (we assume all femto users have the same transmission power). Otherwise, a user which is not associated to any femto cells is a Macro User (MU) with transmission power P_M. In other words, only the users appearing in the unshaded area in Fig. 3.1 will be MUs. Note that, as shown in Section 3.5, our approach is not limited to such a cell association based on the Euclidean distance as in [21], but still applies to other association strategies such as those based on the maximum received power or the biased association [16, 30, 42].

Here, assuming an interference-limited environment, a general path-loss model is applied to characterize the received SIR for both MBS and FBS in the uplink resource reusing scenario by considering the signal's power attenuated with distance [26].

Specifically, the received SIR at the MBS from the MU is

$$SIR_M = \frac{KP_M {d_0}^{\alpha} {d_{MU,MBS}}^{-\alpha}}{I_M}, \tag{3.1}$$

where K is the antenna- and processing gain-related parameter, d_0 is the reference distance, α is the path-loss exponent for the signal propagation within a cell, $d_{MU,MBS}$ is the distance between the MU and MBS, and I_M is the cumulative interference at the MBS from all femto cells,

$$I_M = KP_F \sum_i \left(\frac{d_{FU_i,MBS}}{d_0} \right)^{-\beta}, \tag{3.2}$$

where β is the path-loss exponent for the signal propagation between cells when signals penetrate walls, and $d_{FU_i,MBS}$ is the distance between an FU in femto cell i and the MBS.

Similarly, the SIR at the FBS in femto cell i from its associated FU is

$$SIR_{Fi} = \frac{KP_F {d_0}^{\alpha} {d_{FU_i,FBS_i}}^{-\alpha}}{I_{Fi}}, \tag{3.3}$$

where d_{FU_i,FBS_i} is the distance between an FU and FBS both in femto cell i, and I_{Fi} is the cumulative interference received at this FBS, which consists of two parts: the interference from the MU, I'_{Fi}, and the cumulative interference from all other femto cells except i, I''_{Fi}:

$$I_{Fi} = I'_{Fi} + I''_{Fi}, \tag{3.4}$$

$$I'_{Fi} = KP_M \left(\frac{d_{MU,FBS_i}}{d_0} \right)^{-\beta}, \tag{3.5}$$

$$I''_{Fi} = KP_F \sum_{k \neq i} \left(\frac{d_{FU_k,FBS_i}}{d_0} \right)^{-\beta}. \tag{3.6}$$

where d_{MU,FBS_i} is the distance between the MU and the FBS of the femto cell i, and d_{FU_k,FBS_i} is the distance between the FBS of the femto cell i and the FU in a femto cell other than i.

It is easy to see that the distances between users and BSs play significant roles in (3.1)–(3.6). In the next section, besides obtaining the required distance distributions, we demonstrate our analytical approach for the cumulative interference, SIR, and

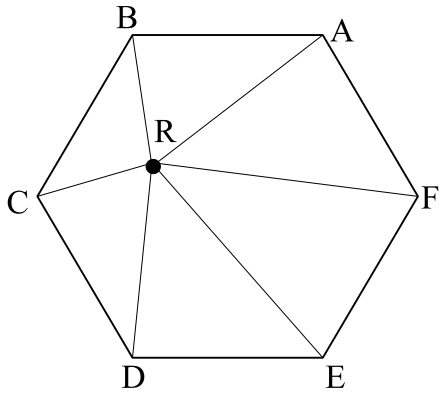

Figure 3.2: Triangulation from the Reference Point.

outage probability.

3.5 Performance Analysis

In this section, we first propose a new approach to obtain the distribution of the distances used in our model, as demonstrated in Section 3.4. With the obtained results, the distribution of the receiving SIR at the FBS and MBS can then be obtained according to (3.1)–(3.6). The investigation on the system outage probability based on the obtained SIR distribution will be shown in Section 3.6.

According to our model, we have the following random variables (RVs), shown in Fig. 3.1, for the distances in (3.1)–(3.6) along with their corresponding CDFs:

SIR at the MBS

(a) $d_{MU,MBS}$ in (3.1): denoted by an RV X, with CDF $F_X(x)$;

(b) $d_{FU_i,MBS}$ in (3.2): denoted by an RV Y_i, with CDF $F_{Y_i}(y_i)$.

SIR at FBS$_i$

(a) d_{FU_i,FBS_i} in (3.3): denoted by an RV W_i, with CDF $F_{W_i}(w_i)$;

(b) d_{MU,FBS_i} in (3.5): denoted by an RV Z_i, with CDF $F_{Z_i}(z_i)$;

(c) d_{FU_k,FBS_i} in (3.6): denoted by an RV U_k, with CDF $F_{U_k}(u_k)$.

Next, we show how to obtain the above CDFs in detail.

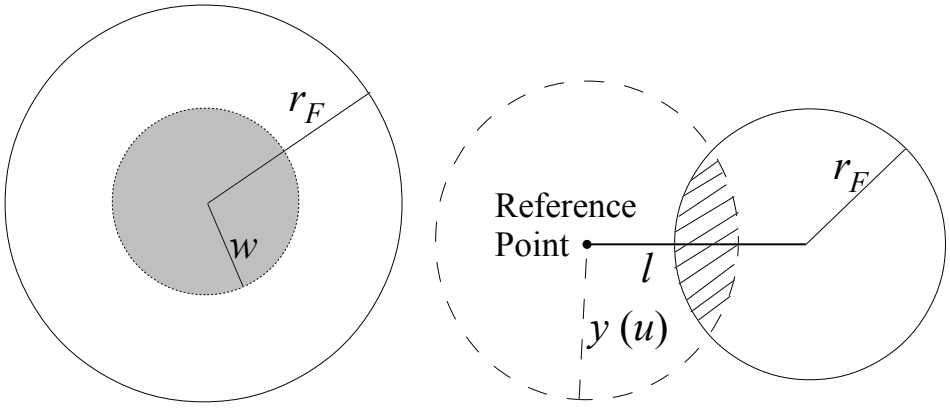

(a) $F_W(w)$ (b) $F_Y(y)$ $(F_U(u))$

Figure 3.3: Demonstration of $F_W(w)$ and $F_Y(y)$ $(F_U(u))$.

3.5.1 Obtaining the Distance Distributions

Here, we explain how the CDFs of the random variables mentioned above can be obtained.

$F_{W_i}(w_i)$

Given that the shape of femto cell i is an irregular polygon, to obtain $F_{W_i}(w_i)$, which is the distribution of the distance from a fixed location (the FBS_i) to a random node (FU_i) in femto cell i, the approach introduced in Chapter 2 is used. According to Chapter 2, the arbitrarily-shaped cell (femto cell i) is first triangulated with respect to the reference point (FBS_i) as shown in Fig. 3.2. Then, the intended distance distribution is obtained by the probabilistic sum of the distance distributions to each of the triangles that constitute the femto cell.

In a simple setting where the femto cell is approximated by a circle, as shown in Fig. 3.3(a), $F_{W_i}(w_i)$ can be given using the area-ratio approach. Denote the radius of the femto cell as r_F. Then,

$$F_{W_i}(w_i) = \begin{cases} \frac{w_i^2}{r_F^2}, & 0 \le w_i \le r_F \\ 1, & w_i \ge r_F \end{cases} . \tag{3.7}$$

$F_{Y_i}(y_i)$ and $F_{U_k}(u_k)$

It is easy to see that $F_{Y_i}(y_i)$ and $F_{U_k}(u_k)$ denote the CDFs of similar distributions of the distance between a random point within a femto cell and an exterior reference

point (MBS or FBS). The distributions differ according to the shape of the femto cell, however, the approach to obtaining them is the same. As explained in detail in Chapter 2, the arbitrary polygon representing the femto cell is first triangulated. Then, the distance distribution is given by the probabilistic sum of the distributions of the distances between the external reference point to each of the triangles constituting the femto cell.

In a simple scenario, assume that the coverage area of femto cell i is approximated with a circle with radius r_F. Let us show how to obtain $F_{Y_i}(y_i)$ in detail. Based on the area-ratio approach, $F_{Y_i}(y_i)$ is the area of the intersection between the circle with radius of r_F and the circle with radius of y_i, divided by the area of the circle with radius of r_F, as shown in Fig. 3.3(b). Therefore,

$$F_{Y_i}(y_i) = \begin{cases} 0, & y_i \leq l - r_F \\ \frac{1}{\pi r_F^2}\left(r_F^2 \cos^{-1}\left(\frac{l^2+r_F^2-y_i^2}{2lr_F}\right)\right. & \\ \quad \left. + y_i^2 \cos^{-1}\left(\frac{l^2+y_i^2-r_F^2}{2ly_i}\right) - \right. & \\ \quad \left. \frac{\sqrt{((l+r_F)^2-y_i^2)(y_i^2-(l-r_F)^2)}}{2}\right), & l - r_F \leq y_i \leq l + r_F \\ 1, & y_i \geq l + r_F \end{cases}, \tag{3.8}$$

where l is the distance between the exterior reference point and the center of the circle with radius r_F. $F_{U_k}(u_k)$ can also be obtained in a similar way, for circular or irregular shapes.

$F_X(x)$

From Fig. 3.1, $F_X(x)$ is the CDF of the distance from the MBS to a random point (MU) within the macro cell, but outside all the femto cells. Let $F_H(h)$ denote the CDF of the distance from the MBS to a random point anywhere within the macro cell, and $F_{C_i}(c_i)$ be the CDF of the distance from the MBS to a random point within the femto cell i. Obviously, $F_{C_i}(c_i)$ is obtained in a similar way as $F_{Y_i}(y_i)$ and $F_{U_i}(u_i)$. Assuming that the area of the irregular-shaped macro cell is $\mathtt{A}$, and the area of femto cell i is $\mathtt{a}_i$, and with the weighted probabilistic sum, we have

$$F_H(h) = \frac{\mathtt{A} - \sum_i \mathtt{a_i}}{\mathtt{A}} F_X(x) + \sum_i \frac{\mathtt{a_i}}{\mathtt{A}} F_{C_i}(c_i) \ . \tag{3.9}$$

To find $F_H(h)$, i.e., the CDF of the distance from a random point within an irregular polygon to an arbitrary given reference point (the MBS), we employ the decomposition and recursion approach based on the distribution of the distance from a random point within an arbitrary triangle to one of its vertices (which has been obtained in Chapter 2), since any polygon can be triangulated. Specifically, the irregular-shaped cell can be triangulated from the location of the MBS, denoted as R, as shown in Fig. 3.2, which produces six triangles, namely, $\triangle RAB$, $\triangle RBC$, $\triangle RCD$, $\triangle RDE$, $\triangle REF$, and $\triangle RFA$. The distribution of $F_H(h)$ is the probabilistic sum of the distance distributions from the MBS to all triangles that constitute the cell.

In a special case, the coverage area of the macro cell is approximated by a regular hexagon with area $\mathtt{A}$, and the MBS is located at the center of the cell. In this case, the hexagon consists of six identical equilateral triangles. Let $F_T(t)$ denote the distribution of the distance from the MBS to a random point within a unit equilateral triangle, which is the same for all the six triangles and can be obtained according to Chapter 2. According to probabilistic sum,

$$F_H(h) = 6\frac{1}{6}F_T(t) = F_T(t). \tag{3.10}$$

Therefore, for a unit regular hexagon, $F_H(h)$ is

$$F_H(h) = \begin{cases} \frac{2\sqrt{3}\pi}{9}h^2\ , & 0 \le h \le \frac{\sqrt{3}}{2} \\ \frac{4\sqrt{3}}{3}\left(\frac{\sqrt{3}}{2}\sqrt{(h^2-\frac{3}{4})}\right. & \\ \quad \left. - h^2\cos^{-1}\left(\frac{\sqrt{3}}{2h}\right)\right. & \\ \quad \left. + \frac{\sqrt{3}\pi}{12}h^2\right)\ , & \frac{\sqrt{3}}{2} \le h \le 1 \\ 1\ , & h \ge 1 \end{cases}. \tag{3.11}$$

Note that the above result under a unit hexagon can be easily scaled by an arbitrary nonzero scalar to obtain the distribution for a hexagon of any nonzero side length [54]. Then, $F_X(x)$ can be finally obtained based on (3.9).

$F_{Z_i}(z_i)$

Similar to $F_X(x)$, $F_{Z_i}(z_i)$ is the distance distribution between an arbitrary interior reference point, denoted as R in Fig. 3.2, to a random point within an irregular-shaped femto cell. Thus, the approach for obtaining $F_X(x)$, can be applied here as

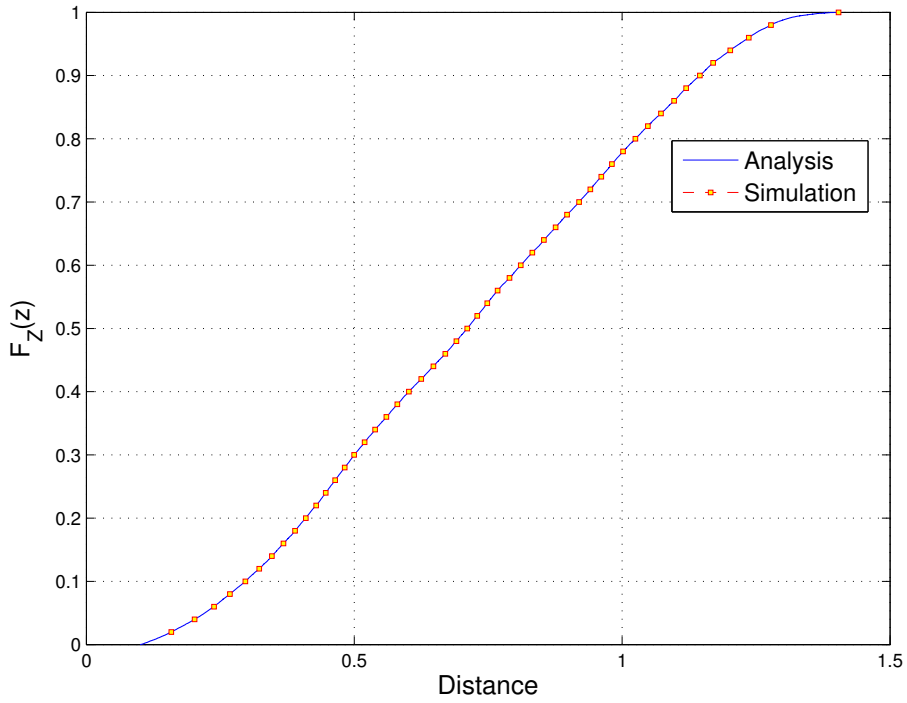

Figure 3.4: Verification of $F_Z(z)$.

well. Assuming that the area of the macro cell is $\mathtt{A}$, and the area of femto cell i is $\mathtt{a}_i$, applying the weighted probabilistic sum, we have

$$F_H(h) = \frac{\mathtt{A} - \sum_j \mathtt{a_i}}{\mathtt{A}} F_{Z_i}(z_i) + \sum_{k \neq i} \frac{\mathtt{a_k}}{\mathtt{A}} F_{C'_k}(c_k) + \frac{\mathtt{a_i}}{\mathtt{A}} F_{W_i}(w_i),$$

where j is an arbitrary femto cell in the macro cell. Thus, $F_{Z_i}(z_i)$ can be obtained.

To the best of our knowledge, there are no existing results of $F_X(x)$ and $F_{Z_i}(z_i)$ in the literature. Therefore, we verify their correctness in comparison with simulations done in Matlab. As $F_{Z_i}(z_i)$ is a more general case of $F_X(x)$, we only present the verification for $F_{Z_i}(z_i)$ in a specified scenario. Specifically, the macro cell coverage is approximated by a regular hexagon with side length 1. There are four femto cells located in the hexagon, each with a circular coverage with radius of $r_F = 0.1$ and centers located at $(-0.3, 0.3)$, $(0.3, -0.3)$, $(0.3, 0.3)$, and $(-0.3, -0.3)$, respectively. The reference point (FBS) is located at $(0.3, -0.3)$. Figure 3.4 demonstrates the CDF of the distances from the reference point to a random point within the hexagon but outside any femto cell. As seen from the figure, our analytical results accurately

match with the simulation results.

3.5.2 Obtaining the SIR Distributions

With the above distance distributions given, the SIR distributions can be obtained according to (3.1)–(3.6). Without loss of generality, we first show the details with the path loss exponent α to obtain the distribution of $d^{-\alpha}$ (the approach is the same for β), which leads to the distributions of the received signal and interference.

Given that the distribution of d is known as obtained in the previous subsection, the change of variable technique can provide the distribution of $d^{-\alpha}$ [6]. Let D be a random variable (representing the distance) with PDF $f_D(d)$ which is defined over $c_1 \leq d \leq c_2$. $D^{-\alpha}$ is introduced as a new variable, D'. Let $D' = D^{-\alpha} = u(D)$, $D = D'^{-\frac{1}{\alpha}} = v(D')$, and $u(c_2) \leq y \leq u(c_1)$. We have

$$\begin{aligned} F_{D'}(d') &= \Pr(D' \leq d') = \Pr(u(D') \leq y) \\ &= \Pr(D' \geq v(y)) = 1 - \int_{c_1}^{v(y)} f_{D'}(d')\mathrm{d}d' \ . \end{aligned}$$

Thus,

$$f_{D'}(d') = F'_{D'}(d') = f_D(v(d')) \cdot |v'(d')| \ . \tag{3.12}$$

Then, we can obtain the distribution of the received signal or interference from one source (e.g., one FU, or the MU).

To obtain the cumulative interference from multiple sources (e.g., several FUs), the convolution operator is used for the probability of the sum of independent random variables.

$$I(x) = \psi^{(n)}(x) \ , \tag{3.13}$$

where $I(x)$ is the cumulative interference from n sources (e.g., n femto cells), and $\psi^{(n)}(\cdot)$ is the n-fold convolution of a given function $\psi(\cdot)$ (distribution of the distance). Note that if the random variables are different, e.g., to sum the interference from an MU and an FU, the convolution theorem can still be applied as they are independent.

Given the distributions of the signal and the cumulative interference, the distribution of the SIR can be obtained. For details please refer to Section 3.6.2.

3.5.3 Further Discussions

Nonuniform Node Distributions

If nodes are non-uniformly distributed in an area, it is possible to look at the area in a different way to convert the nonuniform node distribution to a combination of areas with uniform distributions. In simple words, nonuniform node distribution in an area can be viewed as several uniform node distributions in smaller areas that constitute the original area. As an example, referring to the system model, MUs are distributed in the macro cell polygon but not in the femto cells. Thus, the distribution of the MUs is non-uniform in the entire polygon, however it is uniform in the polygon minus the femto cell holes. Since our approach for deriving the distance distributions can deal with holes, it can also be applied to nonuniform node distributions. In other terms, the approach can be applied to a tiered structure such as the one discussed in this chapter consisting of macro and femto cells.

Cell Association Strategies

In this work, we focused on the association strategy according to the Euclidean distance. However, our approach still applies to other cell association strategies, e.g., association based on the maximum received power, or biased association, if these strategies can be virtually mapped into distances. The received power, for example, is a non-linear function of the distance. Thus, power can be virtually mapped into distance. Furthermore, biased association (maximum received power multiplied by a biased factor) converts the network into cells based on a weighted Voronoi or generalized Dirichlet diagram [16], which can be handled given that our approach for obtaining the distance distributions can be applied to irregular polygons.

Downlink Reuse

In the downlink scenario, the intended receivers are the MU and FUs, in the macro and femto cells, respectively. Thus, the transmitting FBS/MBS can cause interference on the receiving MU/FU, as shown in Fig. 3.5. Specifically, the SIR for the MU is

$$SIR_M = \frac{KP_{MBS}{d_0}^{\alpha}{d_{MBS,MU}}^{-\alpha}}{I_M},$$

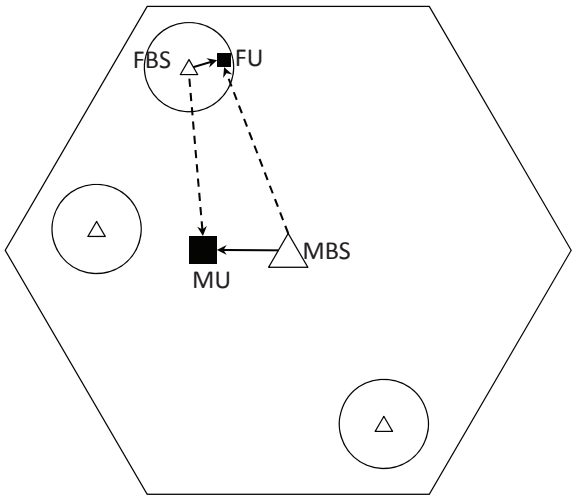

Figure 3.5: System Model: Downlink.

where P_{MBS} is the transmission power of the macro BS. I_M, the cumulative interference at the MU, is

$$I_M = KP_{FBS} \sum_k \left(\frac{d_{FBS_k,MU}}{d_0} \right)^{-\beta},$$

where, P_{FBS} is the transmission power of the FBS (assuming that all FBSs have the same transmission power). The distributions of the distances for $d_{MBS,MU}$ and $d_{FBS_k,MU}$ can be obtained using the approaches explained in Section 3.5.1.

Without loss of generality, to investigate the SIR for a femto user, FU_i, we have

$$SIR_{Fi} = \frac{KP_{FBS} {d_0}^{\alpha} {d_{FBS_i,FU_i}}^{-\alpha}}{I_{Fi}},$$

in which, $I_{Fi} = I'_{Fi} + I''_{Fi}$ is the cumulative interference at the FU_i, where I'_{Fi} and I''_{Fi} are

$$I'_{Fi} = KP_{MBS} \left(\frac{d_{MBS,FU_i}}{d_0} \right)^{-\beta},$$
$$I''_{Fi} = KP_{FBS} \sum_{k \neq i} \left(\frac{d_{FBS_k,FU_i}}{d_0} \right)^{-\beta}.$$

Note that in the downlink case, some of the distance distributions are not independent, such as $d_{MBS,MU}$ and $d_{FBS_k,MU}$. This is because the locations of the BSs

are known in each scenario and thus, the distribution of the distance from different BSs to a random point is correlated. Analyzing the downlink case is one of future directions.

Multiple Macro Cells

The difference between the single macro cell and multiple macro cell scenario lies in the fact that the interference from a neighbor cell MU/FUs needs to be taken into consideration when calculating the SIR for the MBS and FBS. The distribution of the distance from an MU in a cell to an MBS in a different cell can be viewed as the distribution of the distance from an MU to a reference point that is located outside of the cell (the MBS). Similarly, the interference on a femto BS should account for the interference from all MUs in the same and neighbor cells. Depending on the frequency reuse factor in the network, the modeling may be different. Please refer to Section 3.7 where we address multiple macro cell scenarios.

Irregular Cell Shapes

In Section 3.6, we evaluate a network with a hexagonal macro cell and circular femto cells. However, as explained in Section 3.5, our approach applies to scenarios with irregular polygon-shaped macro cells and femto cells, where femto cells do not need to be identical and can have different shapes, sizes, and transmission powers. To analyze the interference and SIR in irregular polygon-shaped networks, the distribution of the distance from a given reference point to a random point inside the cell should be known. This distance distribution can be found based on the decomposition and recursion approach, and based on the distance distributions for arbitrary triangles provided in Chapter 2. Please refer to Section 3.7 where we evaluate a multi-cell network with irregular-shaped cells.

3.6 Performance Evaluation for a Single Macro Cell Network

In this section, we evaluate our analytical approach and provide insights into two important network metrics: cumulative interference and outage probability. First, we show that the numerical results from our analytical approach closely match the

Table 3.1: List of the Parameters

Parameter	Definition
r_F	Radius of femto cells
α	Path loss exponent for indoor-indoor or outdoor-outdoor
β	Path loss exponent for indoor-outdoor or outdoor-indoor
P_F	Transmission power of a femto user
P_M	Transmission power of a macro user
$750 - \delta$	Radius of the exclusive region around the macro base station
N_F	Number of femto cells in a macro cell

simulation results, which can verify the correctness and accuracy of our model. Then, we investigate the effect of several parameters on the performance metrics. All simulations, analytical derivations, and numerical results are done in Matlab.

Considering the system model proposed in Section 3.4, we assume that the macro cell is approximated by a regular hexagon with side length of 750 m [2]. Performance study based on an irregular macro cell is conducted in Section 3.7. The radius of all circular femto cells, denoted as r_F, is 40 m [22]. The femto cells are randomly distributed in the macro cell without overlapping with each other. As explained earlier, our approach does not impose any constraints on the shape of the cell and the results for irregular cells are presented in the rest of this chapter. The path-loss exponent α is used when the signal does not travel through walls, while a different one, β, is used when the signal travels from indoor to outdoor or vice versa to account for the penetration loss due to walls. α is set to 3, and β is 4 [22]. Table 3.1 provides a list of the parameters.

In practical scenarios, the FBSs are located in the locations with poor cellular coverage which are further away from the MBS. From another point of view, in order to limit the cumulative interference on the macro BS, femto cells should be located out of an exclusive region which is modeled as a circle centered at the MBS [37]. The size of the exclusive region is determined by $(750 - \delta)$ m, i.e., the radius of the exclusive region. According to the analysis given in Section 3.5, our approach for obtaining the distribution of the cumulative interference and the SIR, holds no matter the exclusive region exists or not. Furthermore, the shape of the exclusive region or the determination of its size does not affect the application of our approach.

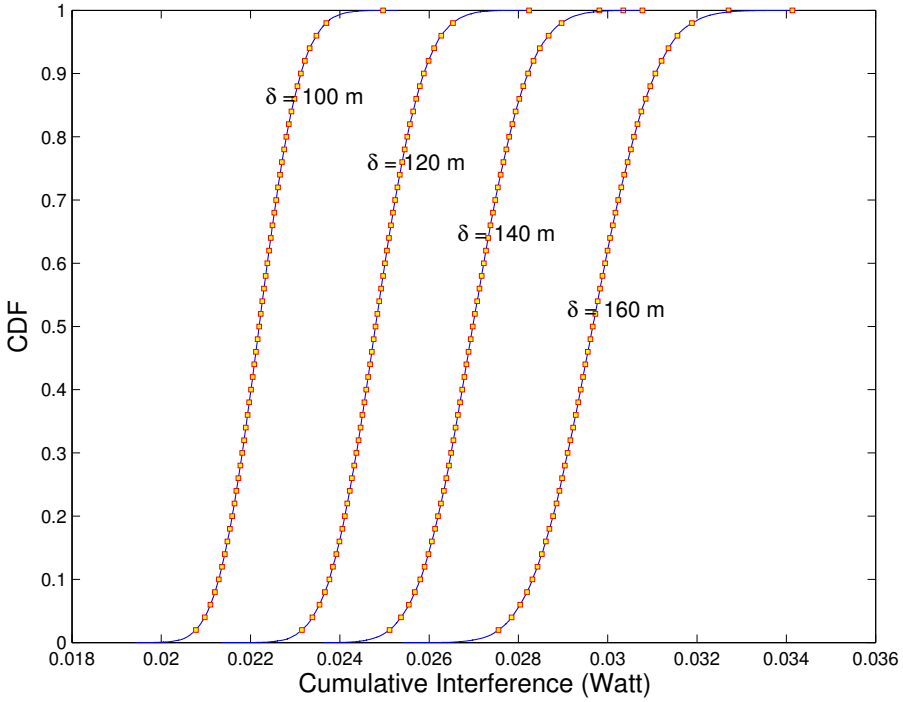

(a) Interference on the MBS w.r.t. δ

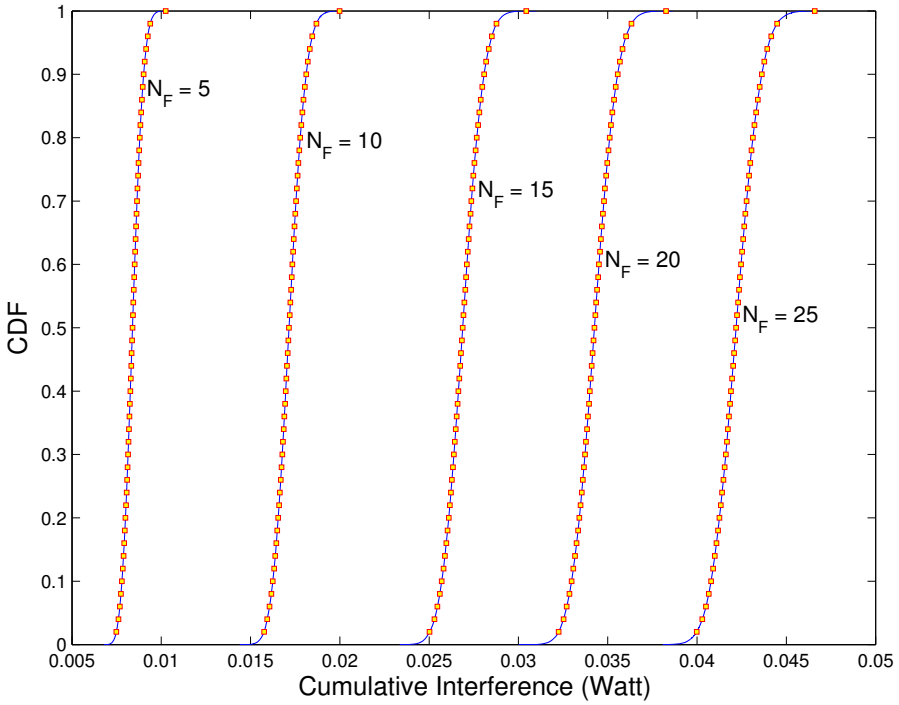

(b) Interference on the MBS w.r.t. the Number of Femto Cells N_F

Figure 3.6: CDF of the Cumulative Interference.

3.6.1 Cumulative Interference

Figure 3.6(a) shows the CDF of the interference at the MBS when δ varies between 100 m and 160 m. P_F is set to 0.7 mWatt. There are 15 femto cells distributed uniformly at random within the macro cell and outside of the guard area. As the figure shows, increasing δ means that femto cells can be located closer to the MBS and thus, they can impose higher interference on the MBS. As a result, the CDF curves corresponding to a larger δ are located on the right-hand side of the CDF curves corresponding to a smaller δ. Moreover, we can observe that the simulation markers and analytical results curves demonstrate a good match.

The effect of the number of femto cells (denoted by N_F) on the total interference at the MBS is shown in Fig. 3.6(b). Here, δ = 140 m and P_F is 0.7 mWatt. The increase in N_F results in the increase in the total interference. This trend can be seen in the figure. Similar to the previous figures, the simulation results are shown by markers on the curves and we can see that they closely match with the analytical results.

3.6.2 Outage Probability

Outage probability represents the probability that the SIR for a transmission is below a specific threshold for a given modulation and coding scheme. In that case, the transmission is considered unsuccessful. Therefore, outage probability is related to the CDF of the received SIR, as shown in Section 3.5.2. Specifically, the received SIR at MBS depends on its distance to the MU (d_C, within the communication range $[d_{\min},\ d_{\max}]$) and the interference from all FUs ($I \in [I_{\min},\ I_{\max}]$). Let $f_I(x_I)$ and $f_C(x_C)$ denote the PDFs of I and d_C, respectively, which can be obtained following the approach explained in detail in Section 3.5. Let the SIR in dB be ζ

$$\zeta = 10\log_{10}(\frac{P_r^{\text{BS}}}{I}), \tag{3.14}$$

where P_r^{BS} is the received power at the MBS from the MU.

Let $S(d_C, I)$ represent the received SIR at MBS given the distances between the MU and the MBS, d_C, and the total interference from the FUs to the MBS, I. Further, let $G_C(\zeta, I)$ be the distance given interference I and received SIR ζ, and $G_I(\zeta, d_C)$ be the interference given distance d_C and the received SIR ζ. Thus, $S(d_{\max}, I_{\max}) \leq \zeta \leq S(d_{\min}, I_{\min})$. Then we obtain the CDF of the received SIR at the MBS:

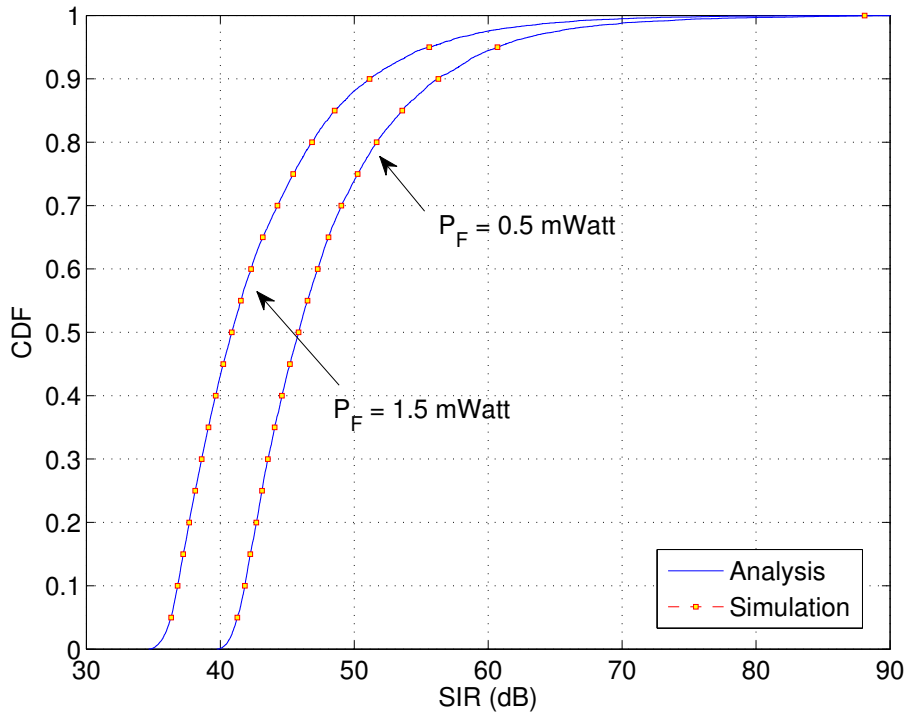

Figure 3.7: Distribution of the SIR at the MBS, with $N_F = 10$, $P_M = 0.15$ Watt, $P_F = \{0.5, 1.5\}$ mWatt.

if $S(d_{\max}, I_{\min}) \leq S(d_{\min}, I_{\max})$, then

$$P(\zeta \leq t) = \begin{cases} \int_{G_I(t,d_{\max})}^{I_{\max}} \int_{G_C(t,x_I)}^{d_{\max}} f_C(x_C) f_I(x_I) \mathrm{d}x_C \mathrm{d}x_I, \\ \qquad \text{if} \quad S(d_{\max}, I_{\max}) \leq t \leq S(d_{\max}, I_{\min}), \\ \int_{d_{\min}}^{d_{\max}} \int_{G_I(t,x_C)}^{I_{\max}} f_C(x_C) f_I(x_I) \mathrm{d}x_C \mathrm{d}x_I, \\ \qquad \text{if} \quad S(d_{\max}, I_{\min}) \leq t \leq S(d_{\min}, I_{\max}), \\ 1 - \int_{I_{\min}}^{G_I(t,d_{\min})} \int_{d_{\min}}^{G_C(t,x_I)} f_C(x_C) f_I(x_I) \mathrm{d}x_C \mathrm{d}x_I, \\ \qquad \text{if} \quad S(d_{\min}, I_{\max}) \leq t \leq S(d_{\min}, I_{\min}). \end{cases} \tag{3.15}$$

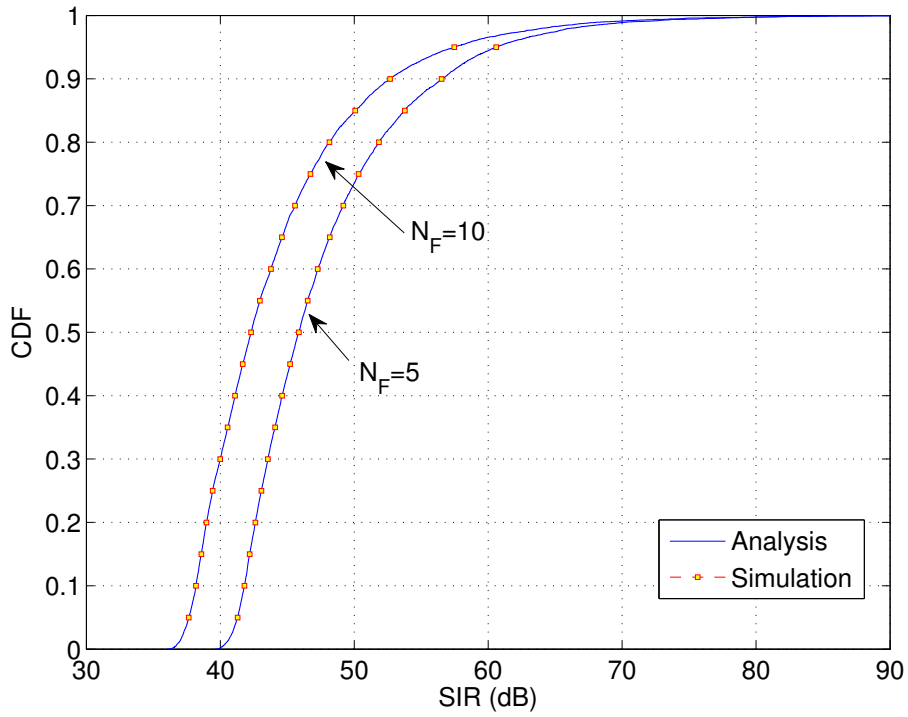

Figure 3.8: Distribution of the SIR at the MBS, with $P_M = 0.15$ Watt, $P_F = 1$ mWatt, $N_F = \{5, 10\}$.

otherwise,

$$P(\zeta \leq t) = \begin{cases} \int_{G_I(t,d_{\max})}^{I_{\max}} \int_{G_C(t,x_I)}^{d_{\max}} f_C(x_C) f_I(x_I) \mathrm{d}x_C \mathrm{d}x_I, \\ \qquad \text{if} \quad S(d_{\max}, I_{\max}) \leq t \leq S(d_{\min}, I_{\max}), \\ \int_{I_{\min}}^{I_{\max}} \int_{G_C(t,x_I)}^{d_{\max}} f_C(x_C) f_I(x_I) \mathrm{d}x_C \mathrm{d}x_I, \\ \qquad \text{if} \quad S(d_{\min}, I_{\max}) \leq t \leq S(d_{\max}, I_{\min}), \\ 1 - \int_{I_{\min}}^{G_I(t,d_{\min})} \int_{d_{\min}}^{G_C(t,x_I)} f_C(x_C) f_I(x_I) \mathrm{d}x_C \mathrm{d}x_I, \\ \qquad \text{if} \quad S(d_{\max}, I_{\min}) \leq t \leq S(d_{\min}, I_{\min}). \end{cases} \tag{3.16}$$

With the number of femto cells $N_F = 10$, the transmission power of the MU $P_M = 0.15$ Watt, and the transmission power of the FU varying from 0.5 to 1.5 mWatt, Fig. 3.7 shows the corresponding distribution of SIR. Intuitively, as P_F increases, the interference from FUs to the MBS increases, and thus, the received SIR at the MBS is low, which increases its outage probability.

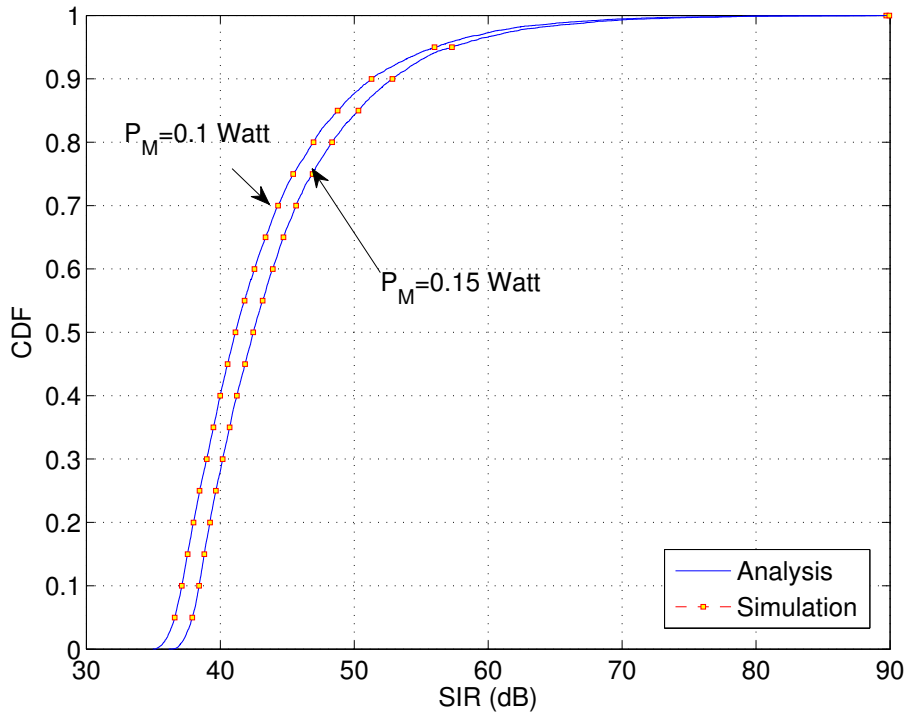

Figure 3.9: Distribution of the SIR at the MBS, with $N_F = 10$, $P_F = 1$ mWatt, $P_M = \{0.1, 0.15\}$ Watt.

Figure 3.8 shows the distribution of SIR with the transmission power of the MU and FUs fixed, namely, $P_M = 0.15$ Watt and $P_F = 1$ mWatt, and the number of the femto cells N_F varying from 5 to 10. Obviously, more femto cells lead to more interference to the MBS, which increases the outage probability of the MBS, as shown in the figure.

Finally, Fig. 3.9 shows the distribution of SIR with $N_F = 10$ and $P_F = 1$ mWatt, and P_M varying from 0.1 to 0.15 Watt. With the transmission power of the MU increased, the received SIR at the MBS will also increase, which correspondingly decreases its outage probability.

All the results in the above figures are in a close match with simulation results and demonstrate the accuracy of our approach. According to our performance studies, the analytical approach proposed in this chapter can be used as a guideline for deploying femto cells, while ensuring a bounded outage probability for the macro cell.

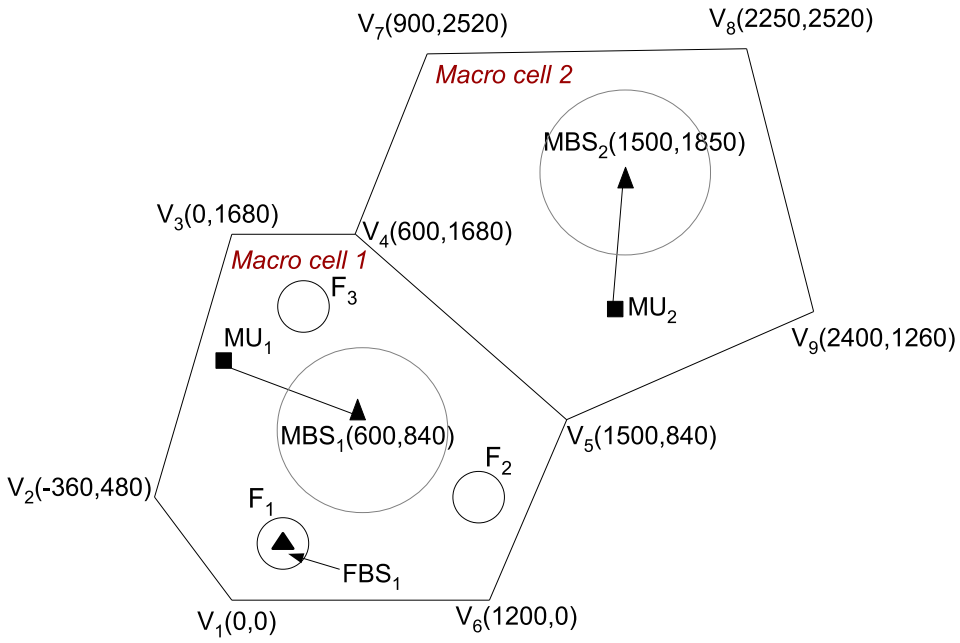

Figure 3.10: A Two-Tier Network Consisting of Multiple Macro and Femto Cells.

3.7 Performance Evaluation for an Irregular Multiple Macro Cell Network

Previous evaluations were based on the assumption of a tiered network consisting of a single regular hexagon-shaped macro cell with multiple femto cells. In this section, we extend our analysis and evaluation for a network with multiple irregular polygon-shaped macro cells as well as multiple femto cells. In this scenario, we analyze and evaluate the cumulative interference, SIR, and the outage probability for a macro BS.

A two-tier cellular network is shown in Fig. 3.10. The network consists of two neighbor macro cells, namely, macro cell 1 and macro cell 2. Note that our approach still applies to networks with more macro cells, with no limitations. Each macro cell has a macro BS namely MBS_1 and MBS_2 for macro cell 1 and macro cell 2, respectively. Furthermore, each macro cell includes multiple femto cells with radius 40 m [22].

Focusing on a multi-cell network, assume that macro cell 1 and macro cell 2 are using different uplink frequency resources. Thus, the uplink transmissions between an MU in macro cell 1 and MBS_1, and an MU in macro cell 2 and MBS_2 occur on different frequency channels, meaning they can happen simultaneously without

interfering with each other. On the other hand, cognitive femto cells in either one of the macro cells are able to choose any of the frequency channels, resulting in possible interference with cellular transmissions in both macro cells.

Without loss of generality, we analyze the SIR at MBS_1 in an uplink scenario.

$$SIR_{MBS_1} = \frac{KP_M {d_0}^{\alpha} {d_{MU_1,MBS_1}}^{-\alpha}}{I_{M_1}}, \tag{3.17}$$

where, I_{M_1} denotes the total interference on MBS_1 and is expressed as the sum of the interference from femto cells in macro cell 1 and macro cell 2, denoted as I' and I'', respectively..

$$I_{M_1} = I' + I'', \tag{3.18}$$

$$I' = KP_F \sum_i \left(\frac{d_{FU_i,MBS_1}}{d_0} \right)^{-\beta} \text{ for femto cells in macro cell 1} \tag{3.19}$$

$$I'' = KP_F \sum_j \left(\frac{d_{FU_j,MBS_1}}{d_0} \right)^{-\beta} \text{ for femto cells in macro cell 2} \tag{3.20}$$

In the above equations, d_{MU_1,MBS_1} can be derived as explained in Section 3.5. Note that d_{FU_i,MBS_1} and d_{FU_j,MBS_1}, both correspond to the distribution of the distance from an FU located randomly within a femto cell to an external reference point, MBS_1, and can be obtained as discussed in Section 3.5. As a result, the distribution of the total interference and SIR can be obtained. Furthermore, the outage probability can be given according to the distribution of the SIR.

In Fig. 3.11, the distribution of the SIR at MBS_1 is investigated. The transmission power of the macro user in cell 1 is 0.15 Watt and that of the femto users is set to 1 mWatt. The number of the femto cells in macro cell 1 is assumed to be fixed at 10.

To understand the effect of the femto cells in macro cell 2 on the SIR at MBS_1, we assume that the number of femto cells in macro cell 2 changes from 0 to 10. Finally, we compare these results with the case where there are 20 femto cells in macro cell 1. As expected and demonstrated in Fig. 3.11, compared with the case where the number of femto cells in macro cell 2 is zero, the outage probability becomes higher when the number of femto cells in macro cell 2 is increased to 10. As femto users become active in cell 2, the interference caused at the MBS is increased which in turn reduces the SIR. The outage probability increases as a result of the decreased SIR.

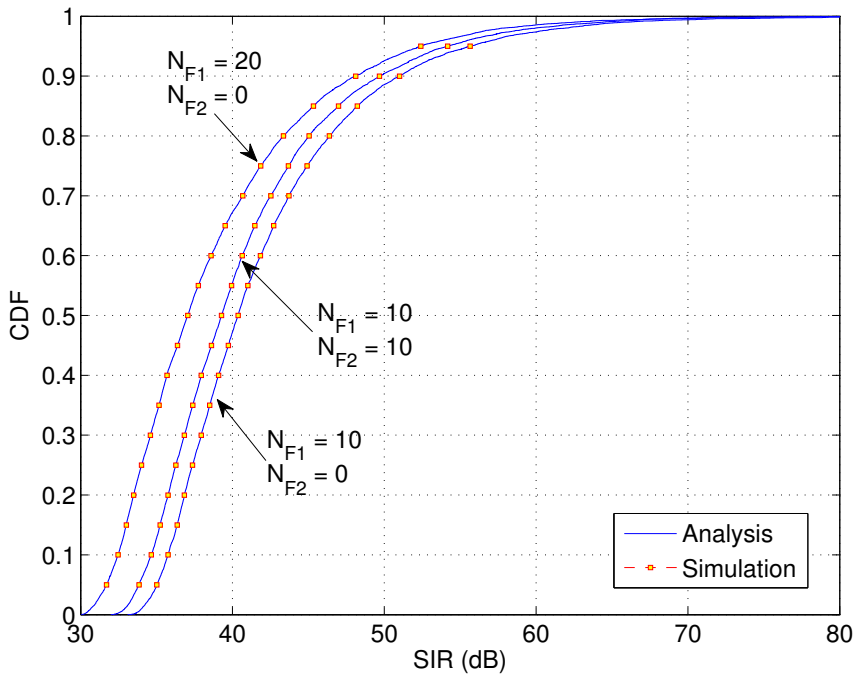

Figure 3.11: Distribution of the SIR at MBS_1, with $P_M = 0.15$ Watt, $P_F = 1$ mWatt, $N_{F1} = 10$, and N_{F2}=$\{0, 10\}$.

However, having 10 femto cells in macro cell 2 has a less negative effect on the SIR at MBS_1 compared to when there are extra 10 femto cells in macro cell 1. This is due to the fact that the interference from femto cells in macro cell 2 is less than that caused by those located in macro cell 1 as their distance to MBS_1 is further. Comparing the curves for $N_{F_1} = 20, N_{F_2} = 0$ and $N_{F_1} = 10, N_{F_2} = 10$, shows this.

In another study, the effect of the transmission power of the femto cells in cell 2 is investigated. The transmission power of the macro user is fixed at 0.15 Watt, while that of the femto users in cell 2 varies between 0.5 and 0.15 mWatt. There are 10 femto cells in each of macro cell 1 and macro cell 2. As observed in Fig. 3.12, as the transmission power of the femto devices in cell 2 is increased from 0.5 to 0.15 mWatt, the SIR at MBS_1 is decreased. Note that the increased transmission power of femto device leads to a higher total interference at the location of MBS_1 which in turn reduces the received SIR for MBS_1 and increases its outage probability.

Note that our approach applies to cases where neighbor macro cells use the same frequency. In that case, the transmissions from neighboring MUs should be taken into consideration as interfering signals.

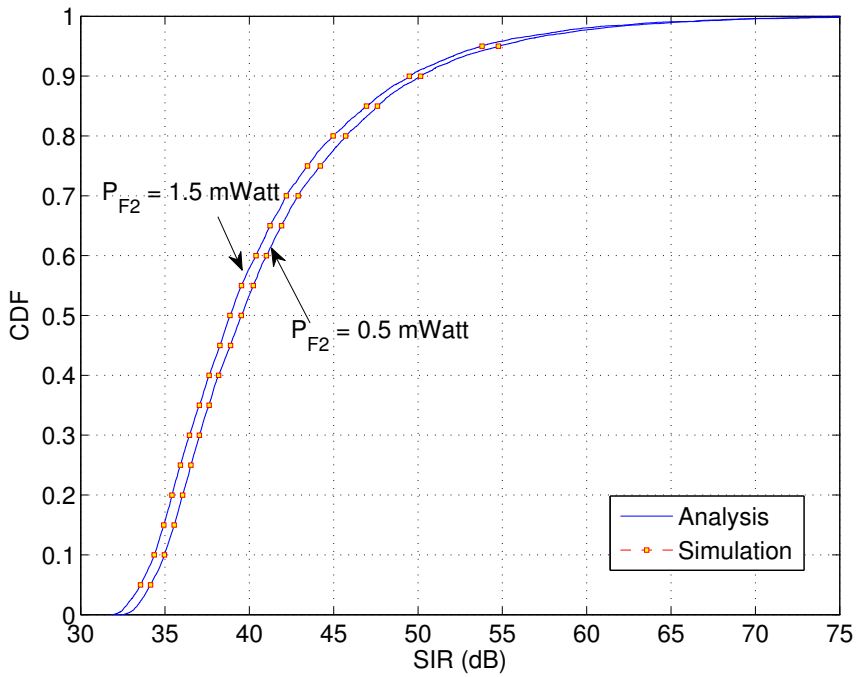

Figure 3.12: Distribution of the SIR at MBS_1, with $P_M = 0.15$ Watt, $N_{F1} = 10$, and N_{F2}=$\{0, 10\}$.

3.8 Performance Analysis and Evaluation for an FBS in an Irregular Macro Cell Scenario

In the previous sections, we demonstrated performance results for a macro BS. In this section, the numerical and simulation results for the distribution of the SIR for a femto BS are presented, from which the outage probability for the FBS can be obtained.

Consider a single macro cell consisting of a macro BS and multiple femto cells. The transmission from a femto user to its corresponding femto BS can potentially interfere with transmissions happening in other femto cells as well as the macro transmission within the macro cell. As a result, the SIR at a given FBS (say FBS_i) can be expressed as below.

$$SIR_{FBS_i} = \frac{K P_F {d_0}^{\alpha} {d_{FU_i,FBS_i}}^{-\alpha}}{I_{F_i}}, \tag{3.21}$$

where,

$$I_{F_i} = I'_{F_i} + I''_{F_i}, \tag{3.22}$$

in which, I_{F_i} denotes the total interference on FBS_i and is the sum of the interference from all other femto cells within the macro cell, and the interference from the MU, denoted as I'_{F_i}, I''_{F_i}, respectively.

I'_{F_i} is a function of the distance between FBS_i and an FU in another femto cell. As explained in Chapter 2, these distance distributions can be easily obtained. Further, I''_{F_i} is a function of the distance between FBS_i and an MU that is located within the macro cell.

Consider macro cell 1 as shown in Fig. 3.10. Assume that a total of 10 femto BSs are within the macro cell. One of the FBSs, denoted as FBS_1 is arbitrarily located at (1154.22,190.98) and nine other FBSs are uniformly distributed at random within the cell. The transmission power of the femto user within the cell of FBS_1 is assumed to be $P_{F1} = 1$ mWatt and that of the femto users in other femto cells is assumed to be $\{1,2\}$ mWatt. The transmission power of the macro user is 0.1 Watt. The macro user is randomly located within the macro cell and outside of all femto cells. Figure 3.13 shows the distribution of the SIR at FBS_1 with respect to the transmission power of the interfering femto cells. As shown in the figure, with the increase of the transmission power of the interfering femto users, the SIR at FBS_1 is less and as a result, the outage probability is higher.

3.9 Conclusions

In this chapter, we considered a two-tier heterogeneous network consisting of multiple irregular polygon-shaped macro cells and multiple femto cells. We first obtained the distance distributions for tiered hierarchical structures consisting of arbitrarily-shaped polygons, for the first time in the literature. Utilizing these distance distributions, we then derived the distributions of the received signal, interference, and SIR for macro base stations, in the uplink resource reusing scenario. Based on the obtained results, the outage probability was thoroughly investigated by varying a series of parameters. The accurate analysis demonstrates the promising potentials of the proposed approach, which we believe can provide meaningful insights and guidelines for the next-generation cellular systems. In the next chapter, we demonstrate how the ap-

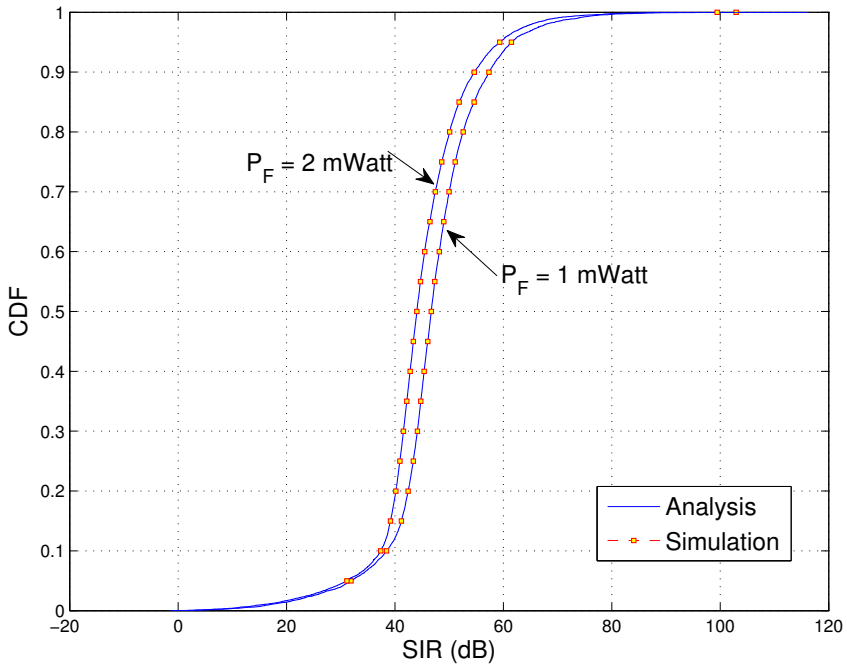

Figure 3.13: Distribution of SIR at an FBS located at (1154.22, 190.98), with P_M = 0.1 Watt, and $P_F = \{1, 2\}$ mWatt.

proach and results obtained in this chapter guide us towards the spectrum allocation for cognitive radio networks.

Chapter 4

Spectrum Allocation and Routing in Ad Hoc Cognitive Radio Networks

4.1 Overview

In Chapter 1, we explained the importance of the interference on the spectrum allocation algorithms. In Chapter 2, we showed how the distance distributions associated with irregular polygons can be obtained. In Chapter 3, we analyzed the performance of a heterogeneous cellular network with irregular cell shapes. In this chapter, we demonstrate how the results in previous chapters can be applied to the spectrum allocation problem. We consider a network consisting of irregular-shaped cells and derive the channel availability probabilities based on the distances between nodes. We show that when the channel availability probabilities are used in spectrum allocation and routing, the delay is decreased and the performance is improved.

4.2 Introduction

The radio spectrum was initially managed by the government agencies, e.g., the Federal Communications Commission (FCC) in the US, in a "command-and-control" manner, where the frequency bands were assigned to authorized users or applications. However, due to the explosive growth of the wireless devices and variation of the services in the past few years, this fixed allocation has led to some problems. For

example, the utilization of some of the licensed spectrum is as low as 15% [4], while transmissions in the Industrial, Scientific and Medical (ISM) bands are facing serious contention, interference, and collision because of the existence of many Bluetooth, WLANs, and WSNs devices, etc., [12, 25].

To mitigate this issue in the fixed frequency allocation, FCC initiated a new spectrum licensing paradigm in 2008 [3], which allows the unlicensed users (Secondary Users, SUs) to more flexibly access the spectrum as long as they do not cause harmful interference to the licensed users (Primary Users, PUs). To use the licensed spectrum, the SUs are required to have cognitive abilities, i.e., they should be able to observe the environment and sense the channels, find the available channels, and utilize them. The secondary users are interchangeably called "cognitive radio users", because of their cognitive capabilities.

The cognitive radio technology, however, has introduced some new challenges. One of the challenges in a network consisting of cognitive radio users is "spectrum allocation". Spectrum allocation includes finding the available channels and appropriately assigning them to the links of the cognitive radio network. From the viewpoint of the PUs, the cognitive users are required to choose channels such that the interference to the PUs stays below a specified threshold. The dynamic environment, however, makes this task very challenging for the cognitive users, as the primary users can come and go without prior notification. Moreover, for the sake of the secondary user performance, channels should be wisely selected for the cognitive network links. This means, for example, channels with a higher availability probability should be chosen. As an example, assume that a cognitive transmitter seeks an available channel before starting to transmit. If this channel selection is performed randomly, the cognitive user may need to sense several channels before an available one is found, since the channel availability is not deterministically predictable. Note that channel sensing and switching between channels are time-consuming. As a result, channels need to be intelligently selected to reduce the sensing time before transmissions. Reduced sensing time will in turn result in reduced end-to-end delay.

We propose to probabilistically measure the channel availability for a node/link. The channel availability probability is then incorporated into the spectrum allocation and routing schemes and can reduce the sensing time before finding an available channel for a transmission, since nodes try to choose the channels that have a higher chance of being available. This probability is based on the activity patterns of the primary users as well as the interference from the secondary network to the primary

and vice versa. Note that interference depends on the distance, due to path loss. Thus, we propose a geometrical probability-based approach by utilizing the distance distributions between nodes to characterize the interference.

The geometrical shape of the network cell is one of the factors that need to be considered in deriving the distance distributions. In the literature, usually a circle or a hexagon is used to approximate the coverage area of a Base Station (BS) in a cellular network [6, 54], while a square is often used to estimate the clusters in ad hoc or sensor networks. However, in real scenarios, the coverage area of a BS can be an irregular shape instead of a circle, hexagon, or other regular shapes. In this chapter, we extend the system model in the previous chapter and assume that the primary network is a Voronoi-structured cellular network consisting of multiple cells with irregular shapes (more details in Section 4.4). The cognitive radio users are also deployed in the same area and communicate with each other opportunistically. As a result, it is critical to use the distance distributions associated with arbitrary polygons for a more realistic performance evaluation. The proposed approach here, applies to regularly-shaped cells, such as hexagons, as well.

Given the approach and results in Chapter 2 and 3, we assume that the distance distributions associated with irregular polygons are known. Using these distance distributions, we obtain the channel availability probability for a cognitive radio user. Then, the link availability probability is obtained for a pair of communicating cognitive radio nodes. Finally, the spectrum allocation and routing are done according to a metric that is derived from the link availability probability.

The simulation results show that the network performance can be improved, in terms of the end-to-end delay, when the proposed metric is considered as the link metric in designing spectrum allocation and routing.

The main contributions of this chapter are twofold. 1) Distance distributions associated with irregular polygons are utilized to obtain the channel availability probability for each cognitive radio node. Then, the link availability probability is obtained for a pair of communicating secondary cognitive radio nodes, according to the primary network activities and the distance distributions between nodes in irregular polygon-shaped network cells. 2) The link metric is incorporated into the spectrum allocation and routing to improve the performance of the cognitive radio network.

4.3 Related Work

In this section, we review the existing work related to spectrum allocation and routing in cognitive radio networks. The related work regarding distance distributions was reviewed in Chapter 2 and is not repeated here.

Spectrum allocation and routing in cognitive radio networks have received considerable attention in recent years [7, 11, 12, 47]. Some work addressed the routing problem in cognitive radio networks assuming that the spectrum allocation has already been done. CAODV (cognitive AODV) [18] is a routing scheme based on the well-known AODV algorithm. In this scheme, it is assumed that the channels are already assigned to the nodes, and thus only a routing algorithm is proposed. Moreover, since the presence of a Common Control Channel (CCC) is not presumed, the Route REQuest (RREQ) messages are broadcast on all the channels, leading to huge overhead. On the other hand, some work has addressed the spectrum allocation problem without considering routing. [17] proposed a spectrum allocation scheme for cognitive sensor networks in which the authors assume that the routes are already known. Since the proposed algorithm is centralized, it may have a huge overhead when applied to large-scale networks.

However, studies have shown that cross-layer designs (where both routing and spectrum allocation are considered) are superior to the decoupled ones (where either spectrum allocation is addressed or the routing) [45]. In [52], the authors proposed a joint routing and spectrum allocation scheme for cognitive radio networks. They proposed a distributed algorithm to improve the route stability of the sessions according to the channel availabilities. However, they have assumed that the licensed channels are available only when the PUs are off. Thus, the interference from the SUs to the PUs is not considered. Another joint routing and spectrum assignment scheme was proposed in [20], where a delay-based metric was considered to determine the effectiveness of routes. This metric includes the switching delay, back-off delay, and queueing delay. In this on-demand routing algorithm, each node chooses a channel according to the previous hop on the route towards the destination. However, the channel availability could change by the time that the source node starts transmission.

Route robustness was addressed in [41] through a joint routing and spectrum assignment scheme, where a level of robustness is guaranteed for some of the routes to be used as the skeleton in the network. In this work, the available channels for each node are assumed to be known, but there are no details on how this channel

availability is obtained. In a robust route and channel selection scheme [51], the route reliability is formulated according to an interference metric as well as the probability that a route is valid. The goal is to minimize the interference to the flows and satisfy the throughput requirements of the flows. However, channels are assumed to be available when the PUs are off. Thus, the interference to the PUs is not considered. In [32], the probability that the capacity of a link is greater than a threshold is calculated according to the interference from the PUs to the SUs. The PUs are modeled as a PPP and the interference from the PUs is assumed to be known as a log-normal distribution. However, the interference from the SUs to the PUs was not considered. A spectrum-aware routing was given in [34]. In this work, the RREQ messages are broadcast on all of the channels. Then, the shortest path is selected according to the delay analysis of paths. This scheme is not scalable to large-sized networks because of the huge overhead. In [50], the total number of neighboring PUs and SUs is estimated by a Bayesian learning method in a centralized manner. These results demonstrate the spectrum availability which is then used in the routing algorithm. However, the learning algorithm requires large volumes of labeled data which is difficult to obtain. Moreover, every SU has to broadcast the channel usage information obtained from sensing the environment, which introduces too much overhead.

Different from the existing work, we propose a distributed joint spectrum allocation and routing algorithm, in which the channel availability probabilities are accurately derived by employing a geometrical probability-based approach. The proposed scheme reduces the number of channel sensing operations, which further reduces the end-to-end delay and of the network.

4.4 System Model

We consider a scenario where there are two coexisting networks: a licensed cellular network (the primary network) and an unlicensed cognitive radio network (the secondary network). In terms of frequency channels, the secondary network users have several choices. They can 1) use the crowded unlicensed ISM bands, where they need to compete with many other unlicensed users such as Wi-Fi users, Bluetooth users, etc., to obtain access to the spectrum; 2) purchase a license for obtaining permission to access a portion of the licensed spectrum, which could be very expensive; 3) opportunistically utilize the licensed spectrum, in which case they can benefit from the

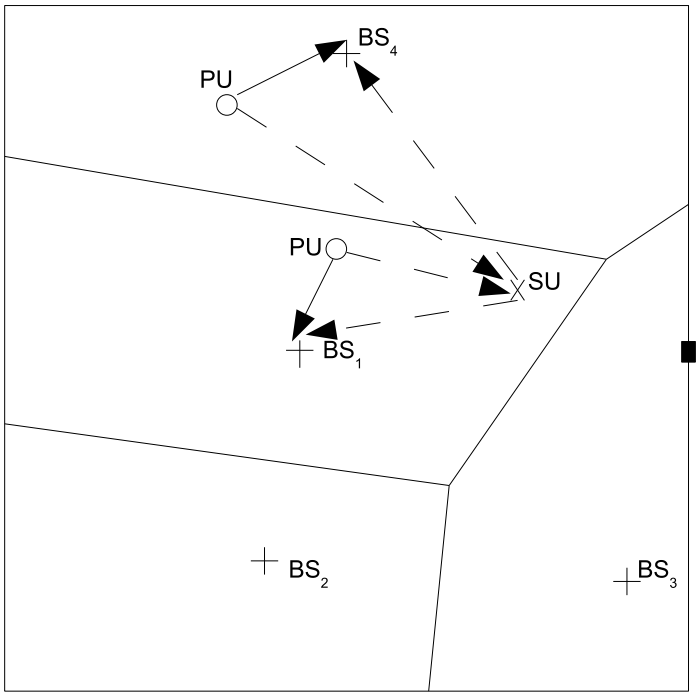

Figure 4.1: System Model.

temporarily unused licensed spectrum (in time, frequency, or space), without spending the cost of owning a licensed spectrum, to achieve high-bandwidth transmissions. Besides the secondary network, the primary cellular network can also benefit from sharing the spectrum with a secondary network by charging the secondary users a relatively low fee. Note that the secondary network will ensure that their transmissions will not interfere with the primary network transmissions. Thus, sharing the spectrum with a secondary network is not only harmless, but also beneficial for the primary network. It is of course beneficial to the secondary network as well.

4.4.1 Primary Cellular Network

We assume that the primary network is a cellular network consisting of multiple cells, where there is a BS in each cell servicing the primary users located in the same cell. In most of the existing work, the coverage area of the BSs in a cellular network was approximated by circles or most recently by hexagons. Circles provide simple analysis, but they lead to either overlap or gap between the cells. However, hexagons provide a more accurate modeling as they provide compactness and coverage efficiency [6,54]. In real world, the shapes of the coverage area of BSs are not circles or hexagons, but

more of irregular shapes, due to many factors regarding the signal propagation. In this chapter, we model the cellular network as a Voronoi diagram [38], to be one step closer to the real world with irregular shapes, where nodes are associated with the BS that is the closest to them. Our proposed approach, however, can be applied to any regular/irregular polygon-shaped cellular network and cells, and is not limited to Voronoi-structured networks.

The cellular BSs are deployed in a square-shaped area, leading to a bounded Voronoi diagram. The BSs are the seeds of the Voronoi diagram. For each BS, a region is defined such that any point in that region is closer to that BS than any other [38]. The primary users are deployed randomly within the square area as shown in Fig. 4.1. Each PU is equipped with a single radio and communicates with the BS located in the same cell, which is the BS that is closest to the PU in terms of the Euclidean distance. Each BS is equipped with multiple radios to accommodate simultaneous communications with the PUs.

Each PU is allocated a specific time slot and a frequency to communicate with the BS. Specifically, the BS can assign a channel to one PU at a time, and to another at a different location and time. Under this scenario, the channels are shared dynamically among the PUs in each cell. Thus, in each cell, over time, each channel is used at random locations, by different PUs. Moreover, we assume that the cells do not share resources and have their own unique resources. In case of resource sharing among neighboring cells, the inter-cell interference needs to be taken into consideration.

4.4.2 Secondary Network

We assume that the secondary network consists of smart grid sensors that are capable of measuring specific metrics and report their measurements to a central sink node. The smart grid sensor network is considered as a possible application, however, other secondary networks could be taken into consideration as well since our approach does not impose any limits on the secondary network topology or application.

The smart grid sensors are deployed randomly within the same area as the cellular network. The nodes are assumed to be stationary, as smart grid sensors have fixed locations. Note that these nodes do not have the limitations of micro-sensor nodes, i.e., they have a larger size and they do not have severe energy limitations. To be realistic, we assume that each node is equipped with only one cognitive radio (cognitive smart grid sensor) that is used for data transmission. Without loss of

generality, the sink is located at the mid-point of the right side of the square area, as shown in Fig. 4.1 with a black square.

The cognitive smart grid sensors transmit short control messages over the CCC to negotiate the establishment of the links and paths. The CCC could be an unlicensed channel or being chosen among the licensed channels in which case it would vary over time and location. Issues related to establishing a CCC among the network nodes have been discussed extensively in the existing work such as [33]. Thus, here, we assume that a CCC already exists and is used by the secondary nodes for negotiation. On the other hand, for data transmissions, cognitive nodes utilize the licensed channels which are the uplink/downlink resources of the primary network and have higher bandwidths and lower utilizations compared with the unlicensed channels.

In this work, it is assumed that the cognitive users are aware of the locations of the BSs (which are often public) and their own locations via GPS or localization techniques. Note that since the smart grid sensor nodes do not have the limitations of the micro-sensors, calculating the location via localization algorithms or being equipped with a GPS device is a reasonable assumption.

Furthermore, we assume that the cognitive secondary network is a time-slotted system, where each time slot is only long enough for one round of channel sensing, link establishment, and data transmission. The channel sensing and negotiation between the two communicating nodes happen at the beginning of the time slot, followed by the data transmission over the established link.

4.4.3 PU/BS Activity Model

The cognitive sensors are allowed to utilize the licensed spectrum as long as they are not imposing harmful interference to the PUs/BSs. Since PUs/BSs are not constantly active, the cognitive users can use the primary channels when the PUs/BSs are inactive. Further, the SUs can use the primary resources even when the PUs/BSs are active but far enough. This means that the signals from the SUs will not cause harmful interference on PUs/BSs.

The BS and PUs activities in the same cell are related to each other, since a PU can be active only when the corresponding BS is active on the same channel, i.e., one is transmitting and the other one is receiving. The ON/OFF model has been widely employed to model the activity of the PUs [33]. Similar to [33], we assume that the BS activity in each of the channels follows an ON/OFF model, where the duration

of the ON and OFF periods are exponentially distributed, similar to other existing work. Thus, the probability of being in ON or OFF state is derived as.

$$P_{ON}(k) = \frac{\beta_k}{\alpha_k + \beta_k} \quad \text{and} \quad P_{OFF}(k) = \frac{\alpha_k}{\alpha_k + \beta_k}, \tag{4.1}$$

where α_k is the probability of transition from ON to OFF for channel k and β_k is that from OFF to ON. Therefore, for each cell, we can describe the BS activity on each channel. Assuming that the secondary nodes only use the uplink resources of the cell, the activity probabilities of a BS BS_b for uplink is

$$Up(BS_b) = \{a_{bk_1}, a_{bk_2}, ..., a_{bk_u}\} \ ,$$

where u is the number of channels for the uplink scenario, and α_{bk_c} ($c \in [1, u]$) is the probability that BS_b is active on the uplink channel k_c.

Here, we focus on the signal attenuation due to path loss, which was introduced in Chapter 3. As mentioned in Chapter 1, shadowing and fading can be easily incorporated in our model if they are not distance-related. Aiming at modeling an irregular-shaped network and considering the path loss model, in order to characterize the interference, the distance distributions associated with irregular polygons are required. These distance distributions can be then used to obtain the distribution of the interference from the secondary transmitter to a PU and from a primary transmitter to an SU. In Chapter 2, we introduced the approach to obtaining such distance distributions. Later in Section 4.5, we explain in detail how the distance distributions can be utilized to find the channel/link availability probabilities, which are then used to help the secondary cognitive radio nodes intelligently choose channels for their transmissions.

4.5 Spectrum Allocation

This section covers how the channel availability probabilities for each channel is calculated by each SU using the distance distributions provided in Chapter 2. Then, the link availability probability is obtained and is incorporated into the routing algorithm.

4.5.1 Channel Availability Probability

The Channel Availability Probability (CAP) denotes the probability that a specific channel is available for a specific SU. Specifically, CAP for a channel depends on the location of the SU, location of the BS, the coverage area of the BS, and the BS activity pattern.

We assume that the secondary network is relatively sparse and in order to avoid collisions, a well-designed MAC protocol will coordinate the SUs that want to use the same channel at the same time. Therefore, the CAPs do not depend on the SU activities, i.e., each SU determines the probability that the channel is available according to the primary network activities.

In a cellular system, the PUs have 2-way communications with their corresponding BSs in uplink and downlink modes. The uplink mode happens when a user transmits to the BS. On the other hand, the downlink scenario takes place when the BS transmits to the PUs. To find the CAPs, we explore the case where the SUs utilize the uplink resources of the primary network.

We adopt the physical interference model [28]. According to this model, for a successful reception (for an SU or PU/BS), the Signal-to-Interference ratio (SIR) at a receiver should be greater than a specific threshold. Note that we consider an interference-limited environment. Thus, considering the simplified path loss model, for a successful transmission from i to j we have

$$SIR(j) = \frac{P_i d(i,j)^{-\alpha}}{I d_0^{-\alpha}} \geq th,$$

where, d_0 is the reference distance, P_i is the transmission power of node i, $d(i,j)$ is the Euclidean distance between the transmitter i and its receiver j, I represents the interference power, and th is the threshold for a successful reception.

A licensed channel can be used by a cognitive user if the primary transmissions do not interfere with the secondary transmissions and vice versa. Most of the existing work, however, focused only on the interference from the primary network to the secondary network (refer to Section 4.3). To be more realistic, we consider both interferences, i.e., the interference from a primary transmission to a secondary receiver, and that from a secondary transmitter to a primary receiver. We assume that each SU could potentially serve as a transmitter as well as a receiver. In other words,

an SU can transmit data to another SU (or the sink) and receive acknowledgement from that node. Thus, we need to ensure that each SU will be able to receive data successfully without severe interference from the primary network, while at the same time, the transmission from the SU should not impose harmful interference to the primary receiver.

In the uplink scenario, two interfering transmissions need to be considered, shown as the dashed lines in Fig. 4.1. One is from the transmitting SU to the BS (the BS is the receiver of the primary signal) and the other is from the transmitting PU to the SU. Based on the physical interference model, in order to ensure that the simultaneous primary and secondary transmissions are successful, the following two conditions should be satisfied

$$SIR(BS) > th_{BS} \ , \ SIR(SU) > th_{SU} \ .$$

For the BS, we have

$$SIR(BS) = \frac{P_{PU} d(BS, PU)^{-\alpha}}{P_{SU} d(SU, BS)^{-\alpha}} \geq th_{BS} \ , \tag{4.2}$$

in which, $d(BS, PU)$ is the distance between the PU and the BS, α is the path loss exponent, and $d(SU, BS)$ represents the distance between the SU and the BS. In other words,

$$d(BS, PU)^{-\alpha} \geq \frac{th_{BS} P_{SU} d(SU, BS)^{-\alpha}}{P_{PU}}. \tag{4.3}$$

Similarly, for the SU we have

$$SIR(SU) = \frac{P_{SU} d(SU, SU)^{-\alpha}}{P_{PU} d(SU, PU)^{-\alpha}} \geq th_{SU} \ , \tag{4.4}$$

in which, $d(SU, SU)$ represents the maximum distance between a pair of communicating SUs. The above equation results in

$$d(SU,PU)^{-\alpha} \leq \frac{P_{SU}d(SU,SU)^{-\alpha}}{P_{PU}th_{SU}}. \tag{4.5}$$

In summary, the two conditions in (4.3) and (4.5) need to be satisfied to guarantee that simultaneous transmissions in the secondary and primary networks are successful. Note that th_{BS}, th_{SU}, P_{SU}, and P_{PU} are assumed to be known values. $d(BS,PU)$ is the distance between the BS and a randomly located PU. Thus, the distribution of $d(BS,PU)$ is the distribution of the distances from a fixed point (the BS) to a random point (the PU) within the same cell. Similarly, the distribution of $d(SU,PU)$ is the distribution of the distances from a given reference point (the SU) to a randomly located point (the PU), where the SU could be an interior/exterior reference point, as shown in Fig. 4.1. These two distributions can be obtained using the approach explained in Chapter 2. Then, given that the distributions of $d(BS,PU)$ and $d(SU,PU)$ are known, the distribution of $d(BS,PU)^{-\alpha}$ and $d(SU,PU)^{-\alpha}$ can be derived using the *change of variable technique*, as described below.

Let D denote the random variable representing $d(BS,PU)$ with PDF $f_D(d)$ defined over $c_1 \leq d \leq c_2$. Remember that $f_D(d)$ is obtained from the approach explained in Chapter 2. Let variable $Y = u(D) = D^{-\alpha}$, thus, $D = Y^{-\frac{1}{\alpha}} = v(Y)$ where Y is defined over $u(c_2) \leq y \leq u(c_1)$. Then,

$$F_Y(y) = \Pr(Y \leq y) = \Pr(u(D) \leq y) = \Pr(D \geq v(y)) = 1 - \int_{c_1}^{v(y)} f_D(d)\mathrm{d}d \ .$$

Therefore,

$$f_Y(y) = F'_Y(y) = -f_D(v(y)).v'(y) \ . \tag{4.6}$$

As a result, the distribution of $d(BS,PU)^{-\alpha}$ can be obtained using (4.6). The distribution of $d(SU,PU)^{-\alpha}$ can be derived in a similar way. Finally, the probability that (4.3) and (4.5) hold, denoted as p_1 and p_2, can be obtained. Since the SUs and the BS require a minimum SIR threshold, we consider the multiplication of p_1 and p_2 as the channel availability probability. Considering the activity of BS_b, channel k is available for SU_i with the following probability

$$p_{ik} = (1 - a_{bk}) + \alpha_{bk} p_1 p_2 \ . \tag{4.7}$$

where, p_{ik} denotes the CAP for SU_i on channel k. In other words, channel k is available for an SU in two cases: 1) if the corresponding BS is in state OFF, and 2) if the BS is ON, then the channel is available to the SU only if both SU and BS can reach the minimum required level of SIR for a successful reception when they are active simultaneously.

Note that the distribution of $d(BS, PU)$ is derived from the distance distributions associated with an interior reference point. To obtain $d(SU, PU)$, depending on the location of the SU, the distance distributions associated with an interior/exterior reference point are used. Details on obtaining such distance distributions can be found in Chapter 2.

As an example, consider the network shown in Fig. 4.1 consisting of four BSs. As explained earlier, in order to ensure that the transmitting SU does not cause harmful interference to the BS, (4.3) should be satisfied. In this scenario, P_{SU} is 1 mWatt, P_{PU} is 0.2 Watt, th_{BS} is equal to 10, and the path loss exponent, α, is 2. The activity probability of BSs is assumed to be 0.3. From the distance distribution expressions given in Chapter 2, we find the probability that (4.3) holds for cells 1 to 4, respectively, which results in $\{0.3350, 0.8409, 0.6183, 0.4271\}$. As seen in Fig. 4.1, BS_2 and its cellular users are further away from the SU compared to other BSs and cellular primary users. Thus, in the case of this example, the probability of finding the channel, corresponding to BS_2, available is higher than other channels. Note that all these results depend on the location of the SU and the BSs. In the same way, the probabilities can be obtained according to (4.5).

The obtained CAPs will be further used to obtain the link availability probabilities and the path weight, which are explained in detail in the rest of this section.

4.5.2 Channel Lists

After finding the CAPs according to the approach explained in Section 4.5.1, each SU records the channel index along with its CAP, for all channels, in a list called the *channel list*. The channel list is sorted in descending order of the CAPs. The channel lists are expected to be different for different SUs (because of their different locations), but similar for the ones that are geographically located close to each other.

Specifically, the channel list for SU_i, denoted as $A(i)$, is defined as below,

$$A(i) = \{(k_1, p_{ik_1}), (k_2, p_{ik_2}), (k_3, p_{ik_3}), \cdots, (k_C, p_{ik_C})\} \ ,$$

where C denotes the number of channels, and p_{ik} shows the probability that channel k is available for node i. Note that $p_{ik_1} > p_{ik_2} > p_{ik_3} > \cdots > p_{ik_C}$, meaning that the list is sorted according to the CAPs. In other words, here, k_1 is the channel with the highest CAP for SU_i.

4.5.3 Link Availability Probability

In a cognitive scenario, a link can only be established if there are two nodes within the transmission range of each other that share at least one available common channel. Note that if a channel is available for one node, there is no guarantee that it will also be available for a neighbor node, as the channel availability depends on the locations of the nodes. Therefore, in order to find the common channels, the channel lists of both two nodes of a potential link need to be known.

First, the two end-nodes exchange their channel lists using the CCC. Given that each end-node is now aware of the available channels of the other end-node, they can easily obtain the common channels. Next, the link availability probability is derived, i.e., the probability that a common channel is available for both of the end-nodes of a potential link. Suppose that channel k is available for both nodes i and j who want to establish a link. The probability of availability of channel k at node i is denoted as p_{ik}, and that of node j is assumed to be p_{jk}. The probability that channel k is available for both node i and j is

$$Pr(k \in A(i) \text{ and } k \in A(j)) = \min\{p_{ik}, p_{jk}\} \ . \tag{4.8}$$

Note that the minimum probability for a common channel, $\min\{p_{ik}, p_{jk}\}$, corresponds to the CAP for the node (either i or j) that is located closer to the location of the primary network and thus has a lower availability probability. The channel availabilities for nodes of a link are correlated. For example, if node i is located closer to a cell whose BS is active on channel k and if channel k is available for i, then it is

also available for node j, who is further away from the cell. Thus, $\min\{p_{ik}, p_{jk}\}$ can be viewed as the probability that the common channel k is available for both of the end-nodes, and will be calculated for all of the common channels between the two nodes. Then, the channel with the highest availability probability for both nodes is considered as the link availability probability of the link between the two nodes i and j.

One may argue that the link availability probability might be higher if there exist many common channels each with a low availability probability compared with when there exists one channel with a higher availability probability. For the case where there are many common channels with a low availability probability, the total availability probability might be high, however, the channel switching time and the sensing time could be considerable, as after each sensing failure the cognitive node has to wait until the beginning of the next time slot, as mentioned in Section 4.4. Moreover, given the proposed approach, once the locations of the BSs and their activities are fixed, the link availability probability is rather deterministic. However, should the network topology change, our scheme can quickly adapt to the new environment. For example, consider a cellular network in which cell breathing happens, i.e., the coverage area of the BSs can change over time depending on the number of the cellular users. The overloaded cells reduce their cell size by reducing the transmission power of the BS while the neighbor cells can increase their coverage area to compensate. In this situation, our proposed approach can quickly adapt to the changes and provide the secondary network with the channel availability probabilities. In addition, if the locations of the secondary users are changed, our scheme can capture that and adapt to it as well.

4.5.4 Route Discovery

In event-detecting WSNs, the sensor nodes, who have detected events of interest, generate messages and report the detected events to the sink. Thus, the direction of the data propagation is from the sensor nodes to the sink. Here, our proposed routing scheme is based on this many-to-one communication pattern. In our proposed scheme, once the paths are determined, the updates are only necessary when the network topology or the link availability probabilities change considerably, e.g., when some sensor nodes run out of battery and die. Unlike some existing algorithms such as [18], this feature eliminates the need of performing route discovery for every flow/packet

and reduces the transmission delay. Specifically, in the initialization phase, the sink node broadcasts a *discovery* message on the CCC which is distributed among the sensor nodes. Upon receiving this message the nodes identify their neighbors and the path toward the sink. The *discovery* message initially includes the sink ID and is propagated on the CCC. Besides the sink ID, the message also includes the following fields: 1) the weight of the traveled path; 2) the channel list of the *last* visited hop.

First, consider the nodes that are located one hop away from the sink. The received *discovery* message from the sink has hop count equal to 0. Each receiving node will add its channel list to the message, and update the path weight (shown in the next subsection) and the hop count fields before the message is re-broadcast. The process is similar for other nodes that are further away from the sink. From the received *discovery* message and by examining the hop count field of the message, each node can determine its next hops toward the sink.

4.5.5 Updating the Path Weight

The path weight is chosen such that it reflects both the hop number to the sink and the probability that the links are available. The metric is defined as below which denotes the minimum theoretical delay.

$$\sum \frac{1}{q_i}, \qquad \forall \text{ link } i \text{ along the path} \tag{4.9}$$

where q_i is the probability of availability of link i. This metric in fact corresponds to the expected delay of each path.

Consider the example shown in Fig. 4.2. Node 0 is the sink node. The arrows show the direction of the *discovery* message propagation. The values on the links show the link availability probability. Between node 0 and 1, a common channel with availability probability equal to 0.5 exists, while between node 0 and 2, the link availability probability is 0.3. Node 1 has two paths to the sink. One is the direct path with weight $\frac{1}{0.5} = 2$, and the other is a two-hop path with weight $\frac{1}{0.3} + \frac{1}{0.2} = 8.33$.

Node 3 receives the *discovery* message from node 1. The message includes the weight of the path from node 1 to the sink. Although node 1 has two paths to the sink, it only reports the best path, which is the shortest path (corresponding to the lowest weight). As a result, the next-hop table of node 3 will include an entry for

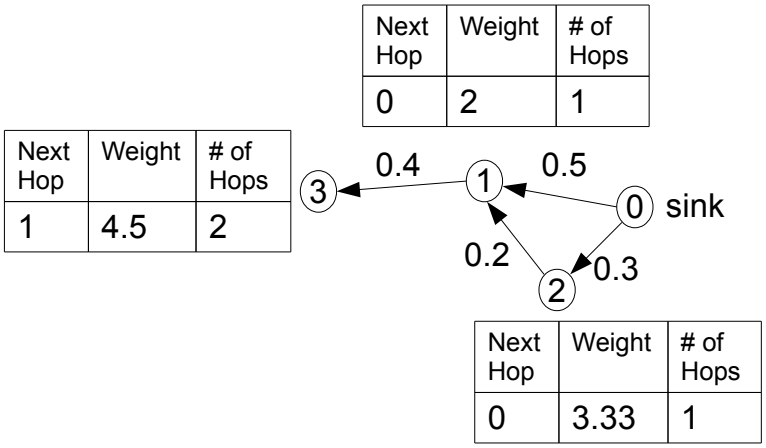

Figure 4.2: Path Weights.

node 1, as the next hop, with weight equal to $2 + \frac{1}{0.4}$, where 2 was reported from node 1.

4.5.6 Data Transmission

In the path discovery phase, the paths from each sensor node to the sink are probabilistically determined. Thus, when forwarding a message, each node refers to its next-hop table and selects the next hop corresponding to the shortest path in terms of the number of hops and the availability probability of the links along the path.

The transmitting node chooses the next hop and the corresponding channel from the next-hop table, and sends an *RTS* message to the receiver through the control channel. In order to ensure the channel availability for both of the nodes of a link, the node closer to the primary network where the channel is being used is responsible for sensing channel and informing the other node of the channel availability. Note that if the channel is sensed busy, the node will wait and sense the channel again at the beginning of the next time slot. Since the chosen channel is the one with the highest availability probability and has the highest chance of being available, the node will sense the same channel in the next time slot. Moreover, this will avoid channel switching. Channel switching is a time-consuming process for cognitive nodes as they may be required to switch to channels over a wide spectrum.

If the transmitting node is also the node performing the sensing, then the node will send the *RTS* message only after the channel is sensed available. In this case,

Algorithm 2 Data Transmission at Node i

```
if queue(i) is not empty then
    choose the first packet in the queue
    find the next hop (j) and corresponding channel (k)
    if i is closer to BS(k) then
        sense k until it is available
        send RTS message to j
    else % if node j is closer to the BS(k)
        send RTS
        wait for CTS from j
    end if
    start transmission once CTS is received
end if
if RTS received from another node h then
    if i is closer to to BS(k) then
        sense k until it is available
    end if
    send CTS
end if
```

after receiving the *RTS* message, the receiver switches to the corresponding channel and sends the *CTS* message. Then, the link can be established. On the other hand, if the receiver is closer to the primary network of the corresponding channel, then the sensing needs to be done by the receiver. The sender transmits an *RTS* message, however, the receiver will reply with a *CTS* only when the channel is sensed available. In that case, after receiving the *CTS* by the transmitter, both nodes switch to the common channel and the link can be established. The algorithm is shown in Algorithm 2. The control messages, such as *RTS*, *CTS*, and *discovery*, are assumed to have small sizes, and thus the unlicensed common channel (e.g., the ISM bands) suffices for their transmissions. However, the data messages that could require higher bandwidths and better QoS are transmitted on the licensed channels.

4.5.7 Spectrum Handoff

Based on FCC rules, cognitive users are required to leave the spectrum when a primary user appears. To accommodate this and similar to [53], we consider a tolerable threshold for the PUs. We assume that each PU can wait for at most one time slot to allow the active SUs to leave the spectrum and then start using the channel. Upon the arrival of a PU, the SU will vacate the spectrum at the end of the current time slot. Since at least the following time slot will definitely be used by the PU, the SU can switch to another channel. If the new channel is available, the SU can use that. However, remember that channel switching is time- and energy-consuming. So, there is a trade-off between switching to a new channel and waiting for the channel with

highest availability to become available again. Thus, in our scheme, if $\lfloor \frac{1}{p_{k_1}} \rfloor = \lfloor \frac{1}{p_{k_2}} \rfloor$, the SU will switch to channel k_2, where channel k_1 is the channel with the best availability probability (requested by PU) and k_2 is the next best channel, p_{k_1} is the probability that k_1 is available for the link and p_{k_2} is that for channel k_2. Note that the condition $\lfloor \frac{1}{p_{k_1}} \rfloor = \lfloor \frac{1}{p_{k_2}} \rfloor$ means that channels k_1 and k_2 have the same expected number of time slots before they are found available. So, an SU only switches to a different channel if the availability probability of that channel for the link satisfies the above mentioned condition.

4.6 Performance Evaluation

In this section, we evaluate the proposed scheme and present simulation results. The performance is evaluated in terms of the end-to-end delay, and the number of sensing trials before an available channel is found. First, the simulation scenario and parameters are explained, followed by the simulation results.

4.6.1 Simulation Setup and Parameters

The simulation is done in Matlab. The simulation scenario is as shown in Fig. 4.1. The primary network consists of four BSs within an area of 1000×1000 m^2. If the area is evenly divided among the BSs, this setting corresponds to a 500×500 m^2 coverage area for each BS, which is a reasonable assumption. The BSs are randomly distributed within the area and the Voronoi cells are found for each BS. The Voronoi cells model a homogeneous cellular network. According to the system model explained in Section 4.4, each BS communicates with a randomly located PU on a channel at a given time. We assume that each BS has one channel only, for uplink, and the BSs in neighbor cells use unique resources. Note that if the BS has more resources, i.e., more than one channel, there will be more channels available to the SUs as well, which can improve their performance. Therefore, we only consider the minimum number of channels, i.e., one uplink, for each cell. The corresponding evaluation results suffice to demonstrate the merits of our scheme. Moreover, the transmission power of PUs is assumed to be 0.2 Watt [2], and the path loss exponent is 2. th_{BS} and th_{SU} are assumed to be 10. The activity probability of BSs is selected randomly between 0.1 and 0.5.

There are 100 smart grid sensor nodes distributed uniformly at random within

the square area. The transmission power of each node is set to 1 mWatt, and the maximum distance between a pair of SUs is assumed to be 150 m. Flows are originated at random nodes and the destination for all flows is the sink node.

The sensor nodes who detect an event, generate data packets and transmit them towards the sink. The path discovery proposed here is the Shortest Path Routing (SPR) algorithm considering the link availability probability. The link availability probability can be translated into the number of time slots required for sensing before the corresponding channel is found available. Each experiment in this section is done 100 times over different topologies and the average results are recorded. 100 packets are transmitted in each experiment.

We incorporate the proposed link metric in the shortest path algorithm in order to find the routes from SUs to the sink. The proposed scheme is compared with the shortest path routing as well. In the shortest path routing algorithm, nodes are not aware of the channel availability probabilities. Thus, in order to establish a link, the nodes choose a random channel to sense. If the channel is not available, they will wait until the beginning of the next time slot to sense a random channel again. The average delay is also compared with the expected delay from the theoretical path weights as introduced in Subsection 4.5.4, corresponding to the minimum transmission delay. In other words, the paths are selected according to the link availability probabilities such that the path has an overall high availability probability. This in turn can reduce the end-to-end delay. Note that before each transmission, the sender needs to sense the intended channel to ensure it is not currently utilized by the primary network. Given the link availability probabilities according to the proposed scheme, the sender senses the channel with the highest availability probability. However, without this knowledge, the sender is required to potentially sense several channels until an available one is found, since the knowledge of the channel availability probability is not available. Thus, our proposed scheme can reduce the sensing delay considerably.

Figure 4.3(a) shows the average delay per packet. The data flows are generated at random sensor nodes, 2 to 10 hops away from the sink. The delay of each packet is measured from the time when it is generated at the source until it is received by the sink. The flow rate is 0.2 pkt/slot. The results labeled as "Minimum Delay" represent the theoretical shortest path delay without considering the queueing delay, as the metric introduced in Section 4.5.5. The "Probabilistic" results demonstrate the results from the proposed scheme. As shown in the figure, the delay is increased as the number of hops is increased. The figure suggests that the proposed scheme

performs very close to the lower bound when the flow rate is low, as in this case the queuing delay in the relay nodes is negligible. The proposed scheme significantly outperforms the SPR scheme.

Figures 4.3(b) and 4.3(c) show the average delay for flow rate equal to 0.5 and 1 pkt/slot, respectively. All of the three figures shown in Fig. 4.3 demonstrate the same trend. We observe that the average delay increases as the flow rate is increased. The reason is that with a higher rate, more packets accumulate in the queues and thus the queueing delay is increased. This also explains why the difference between the proposed scheme and the lower bound increases with the rate.

Considering our scheme for each specific rate, we observe that the delay increases with the number of hops due to the increase of the queuing delay in the relay nodes. Moreover, considering each hop, the delay is larger for higher rates. The increased rate leads to a higher queueing delay that makes the average delay larger.

Figure 4.4(a) shows the number of unsuccessful sensing trials vs. the number of hops from 2 to 10, for both the proposed scheme and the SPR scheme. As expected, the number of unsuccessful sensing trials for the proposed scheme is much lower than that of the SPR scheme, as in the proposed scheme, sensor nodes wisely choose the channel that has the highest probability of being available. This decreases the number of sensing trials which in turn decreases the delay. In the SPR scheme, a channel is randomly selected to be sensed. Compared with the proposed algorithm, it requires a higher number of sensing trials in order to find an available channel. Another observation is that the number of unsuccessful sensing trials for both schemes increases with the increased hop count. This is because the process of finding an available channel has to be finished for each hop, and a larger number of hops leads to a higher number of unsuccessful sensing trials.

We also calculate and plot the ratio of the number of unsuccessful sensing trials to the total number of sensing trials in Fig. 4.4(b), where we observe a huge difference between the proposed scheme and the SPR algorithm, which further demonstrates the merits of our scheme.

4.7 Conclusions

In this chapter, we proposed a geometrical probability-based approach for spectrum allocation in cognitive radio networks. We used the distance distributions associated with arbitrary polygons. Given the distance distributions derived in Chapter 2,

networks with irregular/regular cell shapes can be easily modeled. Assuming that the cognitive radio network coexists with a Voronoi-structured cellular network and according to the activities of the cellular network base stations, the channel availability probabilities for each cognitive user are derived, which are later incorporated into the spectrum assignment and routing. Our proposed spectrum allocation scheme considerably reduces the sensing delay.

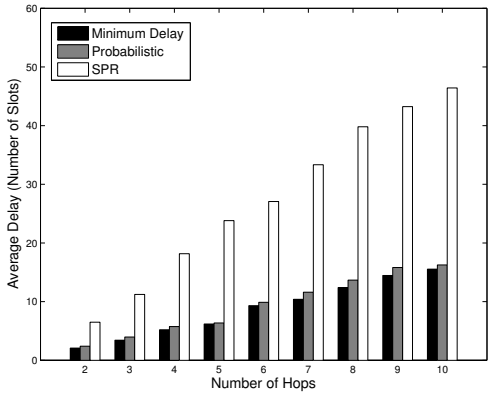

(a) Flow Rate=0.2 pkt/slot

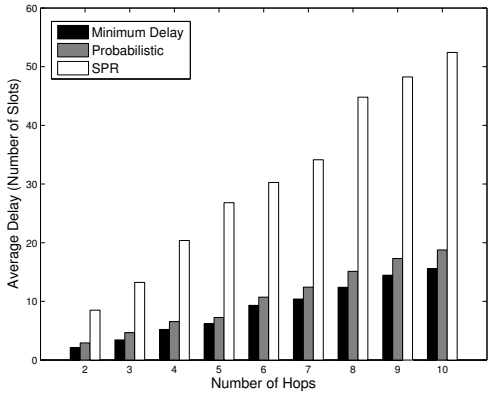

(b) Flow Rate=0.5 pkt/slot

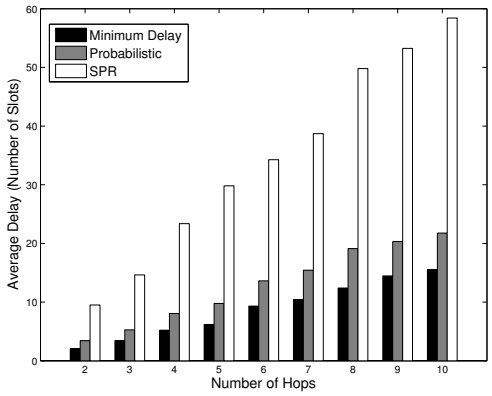

(c) Flow Rate=1 pkt/slot

Figure 4.3: Comparison of the Average Delay among Three Schemes.

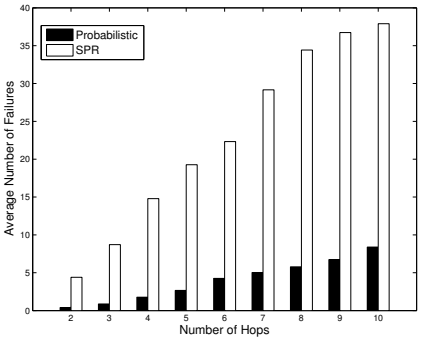

(a) Average Number of Unsuccessful Sensing Trials

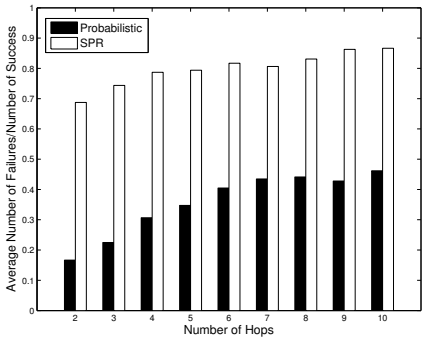

(b) Average Ratio of the Number of Unsuccessful Sensing Trials to the Number of Total Sensing Trials

Figure 4.4: Failures in Sensing.

Chapter 5

Conclusions and Future Work

5.1 Conclusions

In this dissertation, we investigated three important problems ranging from a mathematical tool related to obtaining distance distributions in irregular polygons to interference and performance analysis as well as spectrum allocation and routing for cognitive radio networks. Motivated by the importance of modeling wireless network regions shaped as irregular polygons, for the first time in the literature, we proposed a simple yet efficient and generic scheme to obtain the distribution of random distances associated with irregular polygons. Specifically, assuming that the wireless nodes are distributed within an irregular polygon-shaped network region, we derived the distribution of the distances between an arbitrary given reference point to a random point within the irregular polygon. We proposed a decomposition and recursion approach which simplifies the problem of obtaining the distance distributions associated with arbitrary triangles. Our proposed approach does not impose any limitations on the shape of the polygon or the location of the reference point. In other words, the polygon can be any irregular polygon, either convex or concave, and the arbitrary reference point could be located inside or outside of the polygon. This important mathematical tool facilitates modeling and analysis of wireless networks with irregular cell shapes and we anticipate that it will have a considerable impact on the wireless communications and networking research society.

Utilizing the distance distributions associated with arbitrary polygons and aiming at getting closer to modeling realistic wireless networks, in the rest of this dissertation, we focused on the modeling and analysis of cognitive wireless networks with irregu-

lar polygon cell shapes. First, we considered a heterogeneous cellular network with irregular-shaped cells coexisting with cognitive femto cells. Using the distribution of the distances associated with irregular polygons, as derived in this dissertation, we analyzed the cumulative interference on the base stations. Further, the distribution of the signal-to-interference ratio was obtained from which the outage probability was characterized. The modeling and analysis of heterogeneous networks with irregular cell shapes using distance distributions was the first attempt in the literature and we believe our approach and results will attract future research effort.

Later on, the tools, approaches, and results obtained so far were applied to address the important issue of spectrum allocation and routing in wireless cognitive radio networks. Considering an ad hoc cognitive radio network where nodes are distributed in irregular-shaped cells, the spectrum allocation and routing problems for multi-hop transmissions were discussed. Since the interference plays an important role in spectrum allocation in cognitive radio networks, we used the distance distributions derived in this dissertation to characterize the interference and signal-to-interference ratio, from which cognitive users are able to probabilistically determine the availability of each licensed channel. The link availability probability was obtained from the channel availability probabilities. Finally, based on the link availability probability, a path metric was proposed that takes into consideration the expected time required to deliver a successful message over multiple hops from a source to a destination. Simulation results showed improved end-to-end delay in a cognitive radio network when the proposed routing metric was applied.

5.2 Future Directions and Ideas

In this section, we provide directions and ideas for future research work beyond the scope of this dissertation. The plans and ideas revolve around the distance distributions and their applications in interference analysis, performance analysis, spectrum allocation, and routing in wireless networks.

5.2.1 Distance Distributions Associated with Irregular Shapes

Modeling and analysis of real-world wireless networks provides valuable insights into their performance and helps service providers plan their network for maximum efficiency and profit. Due to physical phenomena, such as path loss, fading, shadowing,

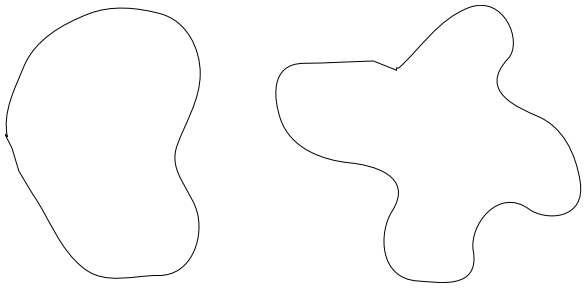

Figure 5.1: Non-polygon Complex Geometries.

etc., that affect wireless signal propagation, the coverage area of a node where its transmitted signal can be received and decoded successfully is not a regular geometric shape. However, due to available mathematical tools, the researchers used disks or other simple regular polygons for modeling this coverage area. In this dissertation, we proposed an efficient and simple scheme that can obtain the distance distributions associated with irregular polygons, from an interior or exterior arbitrary reference point. In addition to our results, in order to be able to model and analyze more complicated scenarios, it would be desirable to obtain distance distributions associated with shapes that are closed curves, i.e., not consisting of edges that are straight line segments. Currently, our proposed scheme cannot obtain the distance distributions associated with this type of complex irregular geometries, unless they are approximated with polygons. Figure 5.1 shows examples of such complex non-polygon shapes.

5.2.2 Extensions on Performance Analysis of Wireless Networks

In Chapter 3, we modeled and analyzed a cognitive femto network coexisting with a multi-cell primary network. Our analysis did not have any limitations on the number of the femto or primary cells, their locations, and their shapes as long as they were polygons.

As mentioned in Chapter 3, the performance analysis of a two-tier cellular network in the downlink scenario can be addressed in future research work. Further, power control for uplink resource reusing scenario can be added to our model.

Furthermore, besides cognitive femto cells, other kinds of nodes, with different network structures, can be assumed to coexist with the cellular network. As an example, Device-to-Device (D2D) communications have been introduced to address the inefficiencies in cellular networks, where the edge users can directly communicate with

each other instead of having their messages relayed through the base station. With the increasing interest in D2D communications, it would be important to accurately analyze the performance of D2D networks, in terms of interference and outage probability and other important performance metrics, using the distance distributions proposed in this dissertation.

5.2.3 Applications in Cognitive Radio Networks

Since the emergence of cognitive radio networks, many important practical issues were introduced that require research efforts. In this dissertation, we focused on the spectrum allocation and routing, however tools and schemes developed in the research work presented in this dissertation can be applied to address other issues as well.

The rendezvous problem in cognitive radio networks happens when two cognitive radio nodes are meeting for the first time. Note that at that point, the two nodes need to find a common channel before they can start communicating with each other. However, they are not aware of the available channels at the other side. Therefore, finding a common channel at a common time that would enable two cognitive radio nodes to meet for the first time is a critical problem that is called the rendezvous problem.

Current solutions in the literature include constructing hopping sequences for the two nodes that guarantee the nodes would meet on a common channel at some time in the future. However, since these approaches are designed without assuming any awareness of the other node's available channels, the rendezvous may not happen very quickly.

The time to rendezvous can be improved by considering the channel availability probabilities at the other node. Given that two nodes can rendezvous only if they are physically close to each other, and considering the fact that the channel availabilities are similar for the nodes that are close to each other, channel availability probabilities can be taken into consideration to shorten the number of the channels in the hopping sequence and thus shortening the time to rendezvous.

Bibliography

[1] Cisco visual indexing report [Online]. `http://www.cisco.com/c/en/us/solutions/collateral/service-provider/visual-networking-index-vni/white_paper_c11-520862.html`.

[2] Evolved Universal Terrestrial Radio Access (E-UTRA); Radio Frequency (RF) requirements for LTE pico node B, 3GPP, Tech. Rep. 36.931, Version 11.0.0, Release 11, 2012.

[3] FCC adopts rules for unlicensed use of television white spaces [Online]. `http://www.bespacific.com/mt/archives/019728.html`.

[4] FCC, spectrum policy task force report, FCC 02-155, Nov. 2002.

[5] Polygon area [Online]. `http://mathworld.wolfram.com/PolygonArea.html`.

[6] M. Ahmadi, M. Ni, and J. Pan. A geometrical probability-based approach towards the analysis of uplink inter-cell interference. In *Proceedings of IEEE GLOBECOM*, pages 1–6, 2013.

[7] M. Ahmadi and J. Pan. Cognitive wireless mesh networks: A connectivity preserving and interference minimizing channel assignment scheme. In *Proceedings of IEEE PacRim*, pages 458–463, 2011.

[8] M. Ahmadi and J. Pan. Random distances associated with arbitrary triangles: A recursive approach with an arbitrary reference point. *UvicSpace* ***http://hdl.handle.net/1828/5134***, 2013.

[9] M. Ahmadi and J. Pan. Random distances associated with trapezoids. *arXiv preprint arXiv:1307.1444*, 2013.

[10] M. Ahmadi, F. Tong, L. Zheng, and J. Pan. Performance analysis for two-tier cellular systems based on probabilistic distance models. In *Proceedings of IEEE INFOCOM*, pages 352–360, 2015.

[11] M. Ahmadi, Y. Zhuang, and J. Pan. Distributed robust channel assignment for multi-radio cognitive radio networks. In *Proceedings of IEEE VTC*, pages 1–5, 2012.

[12] I. F. Akyildiz, W-Y. Lee, M. C. Vuran, and S. Mohanty. Next generation/dynamic spectrum access/cognitive radio wireless networks: A survey. *Computer Networks*, 50(13):2127–2159, 2006.

[13] J. G. Andrews, S. Buzzi, W. Choi, S. V. Hanly, A. Lozano, A. CK. Soong, and J. C. Zhang. What will 5G be? *IEEE Journal on Selected Areas in Communications*, 32(6):1065–1082, 2014.

[14] K. B. Baltzis. Analytical and closed-form expressions for the distribution of path loss in hexagonal cellular networks. *Wireless Personal Communications*, pages 1–12, October 2011.

[15] W. Bao and B. Liang. Understanding the benefits of open access in femtocell networks: Stochastic geometric analysis in the uplink. In *Proceedings of ACM MSWiM*, pages 237–246, 2013.

[16] W. Bao and B. Liang. Structured spectrum allocation and user association in heterogeneous cellular networks. In *Proceedings of IEEE INFOCOM*, pages 1069–1077, 2014.

[17] S. Byun, I. Balasingham, and X. Liang. Dynamic spectrum allocation in wireless cognitive sensor networks: Improving fairness an energy efficiency. In *Proceedings of IEEE VTC*, pages 1–5, 2008.

[18] A. Cacciapuoti, C. Calcagno, M. Caleffi, and L. Paura. CAODV: Routing in mobile ad-hoc cognitive radio networks. In *Proceedings of IFIP*, pages 1–5, 2010.

[19] P. Cardieri. Modeling interference in wireless ad hoc networks. *IEEE Communications Surveys & Tutorials*, 12(4):551–572, 2010.

[20] G. Cheng, W. Liu, Y. Li, and W. Cheng. Joint on-demand routing and spectrum assignment in cognitive radio networks. In *Proceedings of IEEE ICC*, pages 6499–6503, 2007.

[21] S.-M. Cheng, W. C. Ao, and K.-C. Chen. Downlink capacity of two-tier cognitive femto networks. *IEEE Transactions on Vehicular Technology*, 61(5):2194–2207, 2013.

[22] W. C. Cheung, T. Q. S. Quek, and M. Kountouris. Throughput optimization, spectrum allocation, and access control in two-tier femtocell networks. *IEEE Journal on Selected Areas in Communications*, 30(3):561–574, 2012.

[23] H. S. Dhillon, R. K. Ganti, F. Baccelli, and J. G. Andrews. Modeling and analysis of K-tier downlink heterogeneous cellular networks. *IEEE Journal on Selected Areas in Communications*, 30(3):550–560, 2012.

[24] H. ElSawy and E. Hossain. Two-tier hetnets with cognitive femtocells: Downlink performance modeling and analysis in multichannel environment. *IEEE Transactions on Mobile Computing*, 13(3):649–663, 2014.

[25] H. G. Goh, K. H. Kwong, C. Shen, C. Michie, and I. Andonovic. CogSeNet: A concept of cognitive wireless sensor network. In *Proceedings of IEEE CCNC*, pages 1–2, 2010.

[26] A. Goldsmith. *Wireless Communications*. Cambridge University Press, 2005.

[27] J. Guo, S. Durrani, and X. Zhou. Outage probability in arbitrarily-shaped finite wireless networks. *IEEE Transactions on Communications*, 62(2):699–712, 2014.

[28] P. Gupta and P. R. Kumar. The capacity of wireless networks. *IEEE Transactions on Information Theory*, 46(2):388–404, 2000.

[29] L. Huang, G. Zhu, and X. Du. Cognitive femtocell networks: An opportunistic spectrum access for future indoor wireless coverage. *IEEE Transactions on Wireless Communications*, 20(2):44–51, 2013.

[30] H.-S. Jo, Y. J. Sang, P. Xia, and J. G. Andrews. Heterogeneous cellular networks with flexible cell association: A comprehensive downlink sinr analysis. *IEEE Transactions on Wireless Communications*, 11(10):3484–3495, 2012.

[31] Z. Khalid and S. Durrani. Distance distributions in regular polygons. *IEEE Transactions on Vehicular Technology*, 62(5):2362–2368, 2013.

[32] H. Khalife, S. Ahuja, N. Malouch, and M. Krunz. Probabilistic path selection in opportunistic cognitive radio networks. In *Proceedings of IEEE GLOBECOM*, pages 1–5, 2008.

[33] B. Lo, I. Akyildiz, and A. Al-Dhelaan. Efficient recovery control channel design in cognitive radio ad hoc networks. *IEEE Transactions on Vehicular Technology*, 59(9):4513–4526, 2010.

[34] H. Ma, L. Zheng, X. Ma, and Y. Luo. Spectrum aware routing for multi-hop cognitive radio networks with a single transceiver. In *Proceedings of EAI CrownCom*, pages 1–6, 2008.

[35] A. M. Mathai. Random distances associated with triangles. *International Journal of Mathematical and Statistical Sciences*, 7(1):77–96, 1998.

[36] A. M. Mathai and G. Pederzoli. Random points with reference to a circle revisited. *Rendiconti del circolo matematico di Palermo, Serie II, Suppl*, 50:235–258, 1997.

[37] M. Ni, L. Zheng, F. Tong, J. Pan, and L. Cai. A geometrical-based throughput bound analysis for device-to-device communications in cellular networks. *IEEE Journal on Selected Areas in Communications*, 33(1):100–110, 2014.

[38] A. Okabe, B. Boots, K. Sugihara, and S. Chio. *Spatial tessellations: Concepts and applications of voronoi diagrams*. Wiley, 2000.

[39] P. Pirinen. Outage analysis of ultra-wideband system in lognormal multipath fading and square-shaped cellular configurations. *EURASIP Journal on Wireless Communications and Networking*, 2006(2):63–63, 2006.

[40] R. Pure and S. Durrani. Computing exact closed-form distance distributions in arbitrarily-shaped polygons with arbitrary reference point. *The Mathematica Journal*, 17, 2015.

[41] C. Shih, W. Liao, and H. Chao. Joint routing and spectrum allocation for multi-hop cognitive radio networks with route robustness consideration. *IEEE Transactions on Wireless Communications*, 10(9):2940–2949, 2011.

[42] S. Singh, H. Dhillon, and J. G. Andrews. Offloading in heterogeneous networks: Modeling, analysis, and design insights. *IEEE Transactions on Wireless Communications*, 12(5):2484–2497, 2013.

[43] S. Srinivasa and M Haenggi. Distance distributions in finite uniformly random networks: Theory and applications. *IEEE Transactions on Vehicular Technology*, 59(2):940–949, 2010.

[44] F. Tong, M. Ahmadi, and J. Pan. Random distances associated with arbitrary triangles: A systematic approach between two random points. *Arxiv preprint arXiv:1312.2498*, 2013.

[45] Q. Wang and H. Zhang. Route and spectrum selection in dynamic spectrum networks. In *Proceedings of IEEE CCNC*, pages 625–629, 2006.

[46] S. Weber, J. G. Andrews, and N. Jindal. An overview of the transmission capacity of wireless networks. *IEEE Transactions on Communications*, 58(12):3593–3604, 2010.

[47] B. Wei and K. Liu. Advances in cognitive radio networks: A survey. *IEEE Journal of Selected Topics in Signal Processing*, 5(1):5–23, 2011.

[48] M. Z. Win, P. C. Pinto, and L. A. Shepp. A mathematical theory of network interference and its applications. *Proceedings of IEEE*, 97(2):205–230, 2009.

[49] J. Yang. Cognitive radios: System design perspective, Ph.D Thesis, UC Berkeley, 2007.

[50] R. Yu, Y. Zhang, W. Yao, L. Song, and S. Xie. Spectrum-aware routing for reliable end-to-end communications in cognitive sensor networks. In *Proceedings of IEEE GLOBECOM*, pages 1–5, 2010.

[51] J. Zhang, F. Yao, Y. Liu, and L. Cao. Robust route and channel selection in cognitive radio networks. In *Proceedings of IEEE ICCT*, pages 202–208, 2012.

[52] H. Zhao, L. Huang, Y. Zhang, and H. Xu. A stable joint routing and spectrum scheduling scheme for cognitive radio ad hoc networks. In *Proceedings of Mobile Ad-hoc and Sensor Networks*, pages 323–329, 2011.

[53] Y. Zhao, M. Song, and C. Xin. FMAC: A fair MAC protocol for coexisting cognitive radio networks. In *Proceedings of IEEE INFOCOM*, pages 1474–1482, 2013.

[54] Y. Zhuang, Y. Luo, L. Cai, and J. Pan. A geometric probability model for capacity analysis and interference estimation in wireless mobile cellular systems. In *Proceedings of IEEE GLOBECOM*, pages 1–6, 2011.

[55] Y. Zhuang and J. Pan. Random distances associated with hexagons. *Arxiv preprint arXiv:1106.2200*, 2011.

[56] Y. Zhuang and J. Pan. Random distances associated with rhombuses. *Arxiv preprint arXiv:1106.1257*, 2011.

[57] Y. Zhuang and J Pan. A geometrical probability approach to location-critical network performance metrics. In *Proceedings of IEEE INFOCOM*, pages 1–9, Orlando, FL, USA, March 2012.

[58] Y. Zhuang and J. Pan. Random distances associated with equilateral triangles. *Arxiv preprint arXiv:1207.1511*, 2012.